Published in final edited form as:
Neuroimage. 2014 January ; 84: . doi:10.1016/j.neuroimage.2013.09.029.

Quasi-periodic patterns (QPP): large-scale dynamics in resting state fMRI that correlate with local infraslow electrical activity

Garth John Thompson[a], **Wen-Ju Pan**[a], **Matthew Evan Magnuson**[a], **Dieter Jaeger**[b], and **Shella Dawn Keilholz**[a,*]

[a]Department of Biomedical Engineering, Emory University/Georgia Institute of Technology, 101 Woodruff Circle, Atlanta, GA 30322 USA

[b]Department of Biology, Emory University, 1510 Clifton Rd NE, Atlanta, GA 30322 USA

Abstract

Functional connectivity measurements from resting state blood-oxygen level dependent (BOLD) functional magnetic resonance imaging (fMRI) are proving a powerful tool to probe both normal brain function and neuropsychiatric disorders. However, the neural mechanisms that coordinate these large networks are poorly understood, particularly in the context of the growing interest in network dynamics. Recent work in anesthetized rats has shown that the spontaneous BOLD fluctuations are tightly linked to infraslow local field potentials (LFPs) that are seldom recorded but comparable in frequency to the slow BOLD fluctuations. These findings support the hypothesis that long-range coordination involves low frequency neural oscillations and establishes infraslow LFPs as an excellent candidate for probing the neural underpinnings of the BOLD spatiotemporal patterns observed in both rats and humans. To further examine the link between large-scale network dynamics and infraslow LFPs, simultaneous fMRI and microelectrode recording were performed in anesthetized rats. Using an optimized filter to isolate shared components of the signals, we found that time-lagged correlation between infraslow LFPs and BOLD is comparable in spatial extent and timing to a quasi-periodic pattern (QPP) found from BOLD alone, suggesting that fMRI-measured QPPs and the infraslow LFPs share a common mechanism. As fMRI allows spatial resolution and whole brain coverage not available with electroencephalography, QPPs can be used to better understand the role of infraslow oscillations in normal brain function and neurological or psychiatric disorders.

Keywords

functional magnetic resonance imaging; blood oxygen level dependent; local field potential; spatiotemporal dynamics; infraslow oscillation; slow wave; quasi-periodic

*Corresponding author. Phone: +1 404-727-2433, shella.keilholz@bme.gatech.edu.
garth@gatech.edu, wpan5@emory.edu, mmagnuson3@gatech.edu, djaeger@emory.edu

1. Introduction

1.1 Background

Functional magnetic resonance imaging (fMRI) using the blood oxygen level dependent (BOLD) signal has been a key tool in understanding how different parts of the brain respond to a stimulus and, since the discovery of functional connectivity in fMRI (Biswal et al., 1995), how activity across different parts of the brain may be coordinated. Using fMRI to measure coordination between brain regions has been growing rapidly in popularity and has been used successfully to detect alterations in functional networks caused by neurological or psychiatric disorders (Garrity et al., 2007; Greicius et al., 2004; Jones et al., 2010; Tian et al., 2006) and is also sensitive to individual variations that are linked to behavioral performance (Albert et al., 2009; Boly et al., 2007; Hampson et al., 2006; Thompson et al., 2012; Waites et al., 2005; Weissman et al., 2006). Despite its widespread use, the neural, glial and hemodynamic bases of these coordinated fluctuations is still poorly understood, and few models have emerged to explain what is being observed with fMRI.

1.2 Quasi-periodic patterns

Analysis techniques that correlate entire fMRI scans reduce complex spontaneous activity to only a few numbers. Therefore, in recent years, there has been a trend towards dynamic analysis of the coordination of the brain (Hutchison et al., 2013) with the intention of better understanding the makeup of functional connectivity. The majority of these studies have focused on correlation between two brain regions in short time windows, assuming that correlated changes are simultaneous between the tested brain regions (Allen et al., 2012; Chang and Glover, 2010; Handwerker et al., 2012; Hutchison et al., 2012; Keilholz et al., 2013; Kiviniemi et al., 2011; Sakoglu et al., 2010; Thompson et al., 2012) and that there is a relatively static delay or canonical hemodynamic response function between the neural electrical events and the observed hemodynamic changes in the BOLD (Chang et al., 2013; Thompson et al., 2013). This type of analysis assumes that either the first brain region directly drives the second, vice versa, or they are both directly driven by a third, untested region. As neural and glial changes would occur on a time scale shorter than can be measured by fMRI, there would appear to be no delay between the correlated signals at different regions. However, these methods do not consider that the measured correlations may be reflecting a snapshot of some large scale, stereotyped pattern that exists in the underlying neural activity, a “spatiotemporal structure.” This possibility would require coordination of very slow activity in the brain, but the existence of such a spatiotemporal structure had been supported by mathematical models (Deco et al., 2011; Honey et al., 2007).

Early experimental evidence of such a spatiotemporal structure was shown by Majeed et al. (Majeed et al., 2009) who investigated functional connectivity in an anesthetized rat model. They observed a wave of activity in the rats’ brains, propagating from ventral and lateral cortex to dorsal and medial cortex. These waves were occasionally periodic with a frequency of about 0.2Hz. However, they were not always detectable by eye and sometimes a single wave was observed, thus the waves were referred to as “quasi-periodic.” These quasi-periodic patterns (QPP) were of interest partially because some of their characteristics closely matched characteristics of known functional networks in the rat. The QPP showed bilateral symmetry while the most studied functional networks are connected interhemispherically and thus also show that symmetry (Biswal et al., 1995; Cordes et al., 2000). In addition, the QPP passed through interhemispheric secondary somatosensory cortex, primary somatosensory cortex and motor cortex, regions of known functional networks in the rodent (Liu et al., 2010; Williams et al., 2010; Zhao et al., 2008). Following the initial visual observation of QPPs (Majeed et al., 2009) an algorithm was developed that

could locate them through averaging together repeating spatiotemporal patterns in a signal (Majeed et al., 2011). This algorithm produced both a “template,” a characteristic single instance of the QPP, and a time course of the strength of the QPP over time. Thus, the templates were useful in comparing QPPs timing and spatial extent across different subjects, while the time course of QPP strength was useful to compare to other physiological signals. Results from this algorithm showed that QPPs are almost constantly present in both humans and rats.

Using the same methods to find them in humans as were used in rats, Majeed et al. found potentially homologous QPP in awake, healthy human subjects not performing any task (Majeed et al., 2011). Similar patterns have since been found in human subjects using other statistical methods (Allen et al., 2012; Grigg and Grady, 2010; Majeed et al., 2011; Majeed et al., 2009) and in rats using different contrast for fMRI (Magnuson et al., 2010). Interestingly, in human subjects these alternating patterns were similar to two well-known networks; the “default mode” and “task positive” networks (Fox et al., 2005; Raichle et al., 2001), which have been implicated in performance on attentional tasks (Drummond et al., 2005; Weissman et al., 2006) and neuropsychiatric conditions including Alzheimer's disease (Greicius et al., 2004) and attention deficit disorder (Tian et al., 2006). In the default mode network in particular, dynamic changes over time have been linked to behavior variation in healthy human subjects (Prado et al., 2011; Prado and Weissman, 2011; Thompson et al., 2012) and to schizophrenia (Sakoglu et al., 2010). This opens the intriguing possibility that the QPPs may reflect time-varying neural activity which is a potential source for the relationships seen between functional connectivity and behavior or disease. However, the neural basis of the QPPs themselves remained poorly understood.

1.3 Infraslow local field potentials

Thus far, there has been little evidence for a neural substrate for the observed QPPs. Shmuel et al. investigated gamma (40-100Hz) frequencies of brain electrical activity in monkeys and reported a wave of activity seen in fMRI that correlated with an electrode in visual cortex (Shmuel and Leopold, 2008), however the findings were controversial (Logothetis et al., 2009) and not replicated in rats (Pan et al., 2011). Other studies have also indicated that the local field potential (LFP) frequencies that are most correlated with the local BOLD signal are not the most predictive of interhemispheric correlation (Lu et al., 2007; Pan et al., 2011); this suggests that BOLD contains distinct contributions from both local spontaneous activity and widespread functional networks. Therefore, the standard methods used to find neural electrical correlates of the BOLD signal may not be well suited to find neural electrical correlates of QPPs.

It has been postulated that the infraslow components (below 0.5 Hz) of electrophysiological recordings play an important role in the coordination of large-scale networks (Birbaumer et al., 1990; Drew et al., 2008; He et al., 2008; Khader et al., 2008). These hypothetically neural frequencies are directly comparable to the frequency range of the spontaneous BOLD fluctuations used to map functional networks; however these frequencies are rarely examined as most *in vivo* neural electrophysiology is limited by electrode materials (Agranovskii et al., 1998; Geddes, 2001, 2003) or amplifier hardware to frequencies above 0.1Hz.

Despite these challenges, a recent study using simultaneous imaging and DC recording (direct current, no highpass filter) demonstrated high correlation between infraslow LFPs and BOLD at a time lag approximating the hemodynamic delay (Pan et al., 2013). While the correlation was localized to the area surrounding the electrodes at the time of peak correlation, other areas of the brain were also highly correlated at different lag times. At sufficiently large lags, many of the same areas alternated to high negative correlation.

Neither of these phenomena had been observed when using band-limited power of higher frequencies (Pan et al., 2011).

Additionally, Pan et al. showed that the LFP signals and the fMRI signals were most similar in specific infraslow frequencies, and that filtering to these frequencies could improve the clarity of the fMRI-LFP correlations. This would suggest that statistical coherence could be used as an empirical filter to find the most accurate fMRI-LFP correlations to better see the spatiotemporal structure.

1.4 A shared mechanism?

The existence of a structure to the correlations seen between infraslow LFP and fMRI suggests that they are potentially related to the QPPs that were previously observed in fMRI alone. It is possible that the QPPs reflect an underlying infraslow change in field potentials, and correlating with the LFP signal (as Pan et al. did (Pan et al., 2013)) and averaging templates over the fMRI signal (as Majeed et al. did (Majeed et al., 2011)) are two different ways of measuring the same phenomena.

In this study we demonstrate that, in the anesthetized rat model, the QPPs (measured with fMRI alone) and the correlations measured between infraslow LFP and fMRI appear to share a common mechanism. Two different anesthetic agents are used in this study; dexmedetomidine and isoflurane. The purpose of this study is not to compare between anesthetic conditions, rather, two anesthesia are used to act as a control against one another because they provide different mechanisms of suppressing wakefulness and affect vasculature in very different ways (see Appendix A).

First, evidence for a common mechanism between QPPs and infraslow LFP-fMRI correlation is demonstrated by visual examination of the infraslow LFP and fMRI correlation pattern (which had not yet been done systematically in this model) and comparing it to previous work done using fMRI alone (Majeed et al., 2009). Second, the spatiotemporal patterns created when infraslow LFP is correlated with fMRI were statistically compared to templates that were generated using the QPP finding algorithm. The two different types of spatiotemporal pattern (from LFP and fMRI, and from fMRI alone) were statistically similar, indicating that they likely share a common source. Third, the infraslow LFP was compared directly to changes in template strength over time.

Because QPPs have also been observed in awake human subjects, the results of the current study are interesting as they imply a possible electrical basis for these patterns in human subjects as well. The neural electrical basis of resting state functional connectivity is still poorly understood, despite its connection to numerous diseases and behaviors. If the hypothesis that part of functional connectivity emerges from a spatiotemporal structure of brain activity is true, then it is necessary to understand the neural or glial basis of this structure. The present study has taken one of the first steps in this direction.

2. Materials and Methods

ParaVision 4.0 was used for BOLD–weighted image acquisition; LFP recording and data processing were performed using custom software written in *MATLAB*.

2.1 Animal preparation and recording

All procedures were approved by the Emory University Institutional Animal Care and Use Committee. Ten rats were anesthetized with isoflurane anesthesia with fine-tip glass microelectrodes (1 - 5 MΩ impedance) implanted into left and right (interhemispheric) primary somatosensory cortex of the forelimb region (S1FL) for simultaneous LFP-fMRI

recording (Pan et al., 2010). Low-frequency recording was enabled by use of direct-current capable amplifiers and silver/silver chloride leads in glass electrodes (Agranovskii et al., 1998; Geddes, 2001, 2003). The procedures used here are described in detail elsewhere (Pan et al., 2013). Data were collected from six rats under 1.3-2.0% isoflurane and eight rats under dexmedetomidine (four of which were also examined under isoflurane). Dexmedetomidine was administered as a subcutaneous bolus injection of 0.05 mg/kg followed by a continuous subcutaneous infusion of 0.1 mg/kg/hour (Majeed et al., 2009; Pawela et al., 2009).

fMRI BOLD data were acquired on a 9.4 T Bruker animal scanner with a volume transmit coil and an approximately 2 cm homemade surface receive coil using gradient-echo echo-planar imaging (EPI) with TR 500ms (2Hz); TE 15 ms; one 2 mm slice; FOV 1.92 × 1.92 cm; 64 × 64 matrix. 1,000 images (approximately 8 minutes) were collected. LFP data were acquired at 12 kHz from left and right S1FL, beginning several seconds prior to MRI acquisition and ending several seconds after. Between two and fifteen combined fMRI/LFP scans were recorded from each rat.

2.2 Data pre-processing

Six rats had data recorded while under 1.3% to 2.0% isoflurane; of these four were transferred to dexmedetomidine anesthesia for recording. Four further rats were transferred to dexmedetomidine anesthesia immediately following surgery with no isoflurane recording, for a total of ten rats. 5-15 scans were recorded for each rat (2-11 isoflurane, 3-15 dexmedetomidine). Physiological parameters were held within normal values under both anesthetics (Body temperature mean 37.0°C ± 0.3°C under isoflurane, 37.1°C ± 0.1°C under dexmedetomidine, breath rate 56.9 ± 6.99 breaths per minute under isoflurane, 84.3 ± 11.3 breaths per minute under dexmedetomidine, mean ± standard deviation).

Regions of interest (ROI) for left and right S1FL were manually drawn against a two dimensional BOLD image using a rat brain atlas for reference (Paxinos and Watson, 2005) as well as an outline of the whole brain. The mean signal over time in the whole brain was calculated and regressed from each voxel (Fox et al., 2009); following this, each voxel was linearly de-trended. For LFP data, artifacts due to scanning, primarily non-saturated decaying oscillations, were removed by creating a noise template on a per-rat, per-scan basis by averaging the period between each TR together (~ 150ms decay, however the entire 500ms period was used for artifact removal). The noise template was then subtracted from the period between each TR. If the signal was saturated by the gradient amplifiers (< 22ms per 500ms), this section of the signal was replaced by a line connecting the two endpoints of the signal where it was saturated (Allen et al., 2000; Pan et al., 2010). See Figure 2 in Pan et al. (Pan et al., 2011) for an example.

Only data recorded at isoflurane levels of 1.7% to 2.0% were used, and only data recorded under dexmedetomidine at least 2 hours after the switch from isoflurane were used. This range of isoflurane levels was chosen as a previous report had observed robust spontaneous fluctuations within a range of 1.8% to 2.0% (Liu et al., 2010). The time change of the BOLD signal under dexmedetomidine is more complex (Magnuson et al., 2010; Majeed et al., 2009; Williams et al., 2010). To summarize, high power at 0.2Hz is observed after two hours. This suggests a stable state with measurable spontaneous oscillations in BOLD. These exclusions resulted in 2-14 scans per rat (2-8 isoflurane, 3-14 dexmedetomidine) and four rats remaining under isoflurane, seven rats remaining under dexmedetomidine.

2.3 Outline of data analysis procedures

First, methods for generating BOLD-LFP correlation from Pan et al. (Pan et al., 2013) are largely followed, except, to improve the visibility of quasi-periodic patterns (QPP), rather than using a square filter located approximately at the frequencies where high coherence was observed, statistically significant areas of the fMRI-LFP coherence profile itself was used as an empirical filter (section *2.4*). This was compared to a standard filter from previous rat studies (Liu et al., 2010) to test for improvement (section *2.5*). The empirical filter produced, as expected, results with lower error (Table I) and was thus used to find the spatiotemporal pattern of correlation between LFP and BOLD.

The LFP signals were correlated with the corresponding BOLD signals at multiple time shifts and at all voxels. This was visualized as movie files (section *2.6*, see supporting information for example movies). The rest of the methods diverge from Pan et al. (Pan et al., 2013). The movie files were visually inspected to determine if the spatiotemporal structure of the LFP and fMRI correlation appeared similar to the QPPs that were observed in fMRI alone (Majeed et al., 2009). The spatiotemporal pattern of LFP and fMRI correlation was referred to as $r_{\text{lfp-bold}}$.

As $r_{\text{lfp-bold}}$ did appear to match the previously observed QPPs, several methods to quantitatively test this were employed. To quantify the spatiotemporal dynamics, an algorithm was run that produced a “template” and a time series of QPP strength over the course of the fMRI run (Majeed et al., 2011) (section *2.7*). This was then compared to either $r_{\text{lfp-bold}}$ or LFP directly; both are outlined in Figure 1.

To compare $r_{\text{lfp-bold}}$ to QPP templates, the templates were all aligned to the first rat and scan's template for that anesthesia. Spatial correlation at every possible frame shift between $r_{\text{lfp-bold}}$ and the template was calculated to give a plot of correlation versus frame shift. This plot was referred to as $r_{\text{lfp-bold-template}}$. Setting the point of highest mean spatial correlation across all rats and scans to be the “zero” frame shift, statistically significant peaks in $r_{\text{lfp-bold-template}}$ were examined to determine if $r_{\text{lfp-bold}}$ and the templates shared common spatiotemporal information. This is described in section *2.8* and shown on the right-hand side of Figure 1.

To compare QPP strength over time to LFP directly, the time course of QPP strength was aligned to the first rat and scan's time course (because of the phase differences of the QPP). Cross-correlation was then calculated between the filtered, preprocessed LFP signal and the aligned strength of the QPP over time, the result was referred to as $r_{\text{lfp-template}}$. Setting the point of highest mean correlation across all rats and scans to be “zero” time shift, statistically significant peaks in $r_{\text{lfp-template}}$ were examined to determine if the LFP and the time changes of the QPPs shared common temporal information. This is described in section *2.9* and shown on the left-hand side of Figure 1.

Thus, through the methods shown in Figure 1, we statistically validate the visual observations shown in Table II. Through analysis of $r_{\text{lfp-bold-template}}$ we demonstrate that the spatiotemporal structure of LFP and fMRI correlations is correlated with QPPs in the same data. Through analysis of $r_{\text{lfp-template}}$ we demonstrate that the infraslow LFP is directly (if weakly) correlated with the timing of the QPP. The visual similarity, supported by statistical significance of correlations, strongly supports that part of the QPP shares a common origin with part of the infraslow LFP, in particular the part that correlates with fMRI.

2.4 BOLD-LFP coherence

The preprocessing described in this paragraph was done only prior to coherence calculation and differs from pre-processing was done for the other analyses (described in section *2.5* and

onward). BOLD and LFP data were quadratically de-trended (Majeed et al., 2011) and set to zero mean. Mean BOLD time courses were calculated for left and right S1FL by taking the mean BOLD signal over time within the respective ROI for those areas. LFP data were resampled to 2Hz to match the BOLD using an anti-aliasing filter ("resample" function in *MATLAB*). S1FL BOLD and LFP data were then both normalized to unit variance, zero mean.

As the BOLD-LFP relationship can likely be modeled by a consistent time shift representing a hemodynamic response to neural activity, we are most interested in frequencies with consistent phase difference between infraslow LFP and BOLD. Therefore, magnitude-squared coherence was calculated using the mscohere function in MATLAB between each electrode's LFP and the BOLD signal at the corresponding S1FL region of interest (the cortex surrounding the electrode). The entire possible range of zero to one Hertz (as BOLD data were 2Hz) was calculated for each scan with 2,000 frequency steps to ensure an adequately smooth result. Mean coherence spectra were calculated for both anesthetic agents by averaging across all rats, all scans and both sides of the cortex.

Based on where significant coherence was observed (see *3.1*), the first large peak appeared to be a good choice for developing an empirical filter to use on infraslow LFP and BOLD. The "first large peak" of the significant (low-frequency, see results) mean coherence was selected as follows; the start point was defined as the lowest frequency local minimum in the mean coherence and the end point was defined as the lowest frequency local minimum in the mean coherence where the mean coherence value was 50% or less than the maximum peak reached in the coherence spectra at frequencies greater than the lowest frequency local minimum.

2.5 Filtering for time-lagged BOLD-LFP correlation

Both a standard and an empirical filter were calculated on a per-anesthesia basis. The first filter was a standard hard-edged Fourier filter with a pass band based on a standard used for isoflurane anesthetized rats (0.005Hz to 0.1Hz, (Liu et al., 2010), p375). The second filter was applied by first calculating the fast Fourier transform (FFT) of the signal. Then, the "first large peak" (see *2.4*) of the mean coherence spectrum was set to minimum zero, maximum one and multiplied by the FFT of the signal at each corresponding frequency. This was done to attenuate frequencies that were not coherent between the two signals. The inverse FFT was applied to the result, and any residual imaginary part of the signal was set to zero. (Note that, while computationally inefficient, the filter was applied as a multiplicand to the complete FFT directly, because a system such as a finite impulse response filter may have created unpredictable edge effects due to the unknown effect of the shape of the empirical filter on phase.) The second filter has the advantage of only assuming that amplitudes of infraslow LFP and BOLD will be similar during time periods where their frequency content is similar; this is because the equation for coherence is similar to the equation for correlation with covariance replaced with cross-spectral density. Use of an empirical filter is also suggested by previous work (Pan et al., 2013).

BOLD data were resampled to 4Hz to facilitate a greater range of phases in templates for pattern-matching (see *2.7*), and LFP data were downsampled to 4Hz (both were done using the "resample" function in MATLAB, which uses an anti-aliasing filter). Both signals had quadratic de-trend performed (Majeed et al., 2011). Each filter was applied separately to all data (BOLD and infraslow LFP for every scan, every rat), then data were normalized to zero mean. As this study is concerned with infraslow LFP-BOLD correlates in matched frequencies, the same filter was applied to the data for infraslow LFP and BOLD in each case.

2.6 Calculation of time-lagged BOLD-LFP correlation: $r_{lfp\text{-}bold}$

Pearson correlation was calculated between each electrode's LFP and the BOLD signal at every voxel for time shifts from −10s to 10s with positive numbers indicating that the BOLD came after the LFP. Results of this calculation are referred to as $r_{lfp\text{-}bold}$. The range of ±10s was selected to be more than sufficient to capture previously observed localized correlations in rats between the simultaneously recorded signals (Pan et al., 2011; Pan et al., 2013) but was set larger so that results would not be biased toward only the expected time shifts. As bursting was in the negative direction, correlation coefficients were inverted. This was because previous work by Pan et al. (Pan et al., 2013) used this convention; it was hypothesized that, since a relationship between positive LFP and positive fMRI has been seen since very early simultaneous models (Logothetis et al., 2001), the LFP-fMRI relationship would also invert when LFP was recorded from a cortical layer where bursting was inverted.

The empirically derived filter was used for all further analysis as it produced more consistent results (Table I). No Fisher transformation or other normalization was used on $r_{lfp\text{-}bold}$, as some data were calculated with an empirical filter which may have had unpredictable effects on such a transform. To account for this lack of normalization, only p values from comparisons to randomized data were used to test for significance and some tests were replicated using median values instead of mean values (see *2.11* and *2.14*).

Movies were created using the “jet” color scale in *MATLAB* and a range of $r_{lfp\text{-}bold}$ between ±0.4 and examining only time shifts of −3s to 10s. A researcher (G. J. Thompson) visually inspected the movies for alternation between positive and negative correlation, as well as propagation from ventral to dorsal cortex, dorsal to ventral cortex, or neither. Example movies are included as supporting information.

2.7 QPP template generation

For a statistical examination of dynamic correlation patterns, templates of inherent QPPs in the BOLD signal were generated for each anesthesia, rat and scan. This also simultaneously generated a time course of sliding correlation with the template, which can be considered template strength over time. The algorithm used to generate these templates is described in Majeed et al. (Majeed et al., 2011); exact parameters and the methods used to align templates relative to each other are described in Appendix B.

2.8 LFP-BOLD correlation versus QPP templates: $r_{lfp\text{-}bold\text{-}template}$

To compare the spatiotemporal distribution of high signal within the frame shifted QPP templates to the spatiotemporal distribution of correlation between infraslow LFP and BOLD, the following analysis was done: Normalized spatial correlation was calculated between aligned templates and $r_{lfp\text{-}bold}$ values to produce a result referred to as $r_{lfp\text{-}bold\text{-}template}$. This was done at all possible frame shifts given the lengths of $r_{lfp\text{-}bold}$ and the template. Maximum normalized spatial correlation between the template and $r_{lfp\text{-}bold}$ was calculated on a per-frame basis using the normxcorr2 function in MATLAB, however only the central (zero shift) correlation was taken in each case as templates and $r_{lfp\text{-}bold}$ are co-registered as they came from the same scan. Correlation coefficients were inverted. $r_{lfp\text{-}bold\text{-}template}$ values were re-centered in terms of frame shift to be relative to their maximum values. A brief summary of these methods is shown in Figure 1.

2.9 Correlation between template strength and LFPs: $r_{lfp\text{-}template}$

To compare the occurrences in time of QPPs to the infraslow LFP signal directly, the following analysis was done: Pearson correlation was calculated between the aligned

template strength time courses and the processed LFP signal in each electrode to produce values referred to as $r_{lfp\text{-}template}$. This was done at time shifts from −20s (LFP signal shifted forward relative to sliding correlation with template) to 20s (LFP signal shifted backward relative to sliding correlation with template). Correlation coefficients were inverted. $r_{lfp\text{-}template}$ values were re-centered in terms of time shift to be relative to their maximum values. A brief summary of these methods is shown in Figure 1. To ensure that the lack of normalization for correlation values would not bias results, $r_{lfp\text{-}bold}$ was also calculated with median instead of mean values used (see *2.11* and *2.14*).

2.10 Estimation of period of autocorrelation series

Results for $r_{lfp\text{-}bold\text{-}template}$ and $r_{lfp\text{-}template}$ that appeared similar to an autocorrelation series of a periodic process had the phase of the hypothetical periodic process estimated. The period of a periodic process can be calculated from the first several peaks of its autocorrelation series by averaging the expected period from each of those peaks. An example calculated from four peaks is shown in Equation 1, where the time shifts of two positive peaks (PPL on the left and PPR on the right) and the time shifts of two negative peaks (NPL on the left and NPR on the right) are known.

2.11 Use of median instead of mean

As normalization was not performed on correlation coefficients (see *2.6*), to validate the methods an additional test was done that did not use mean values but instead used median values (50th percentiles) which are independent of assumptions of the shape of the distribution of data. As the means of correlation values were only taken at the last step, the values calculated for $r_{lfp\text{-}template}$ were used for this test, taken as a median across all rats and scans for each anesthesia and electrode. Identical significance testing was done as was done when a mean was taken (see *2.14*).

2.12 Test of preliminary caudate-putamen electrical recording

As reported in Pan, et al. (Pan et al., 2013), preliminary data has been recorded under the same protocol, with the exception of the electrode being implanted into the caudate-putamen instead of S1FL. The same data are used here as it would be informative to future work to know if the present study can be translated to non-cortical locations.

This datum was subjected to identical pre-processing as the interhemispheric S1FL data, using the empirical filter used in this study for S1FL and dexmedetomidine anesthesia, and had $r_{lfp\text{-}bold}$ and $r_{lfp\text{-}bold\text{-}template}$ calculated on the single scan. The only change made to data processing was use of regions of interest drawn in the left and right caudate-putamen for calculation of the QPP template.

2.13 Power spectrum of template strength versus time

For each anesthesia, rat and scan, a power spectra was calculated on the template strength (time course of sliding correlation with the template). This was done using a Welch spectrum with 1,000 frequency steps, 200s window length and 99.5% overlap. This was done to measure the strongest frequency in each of the of the QPPs being examined.

2.14 Control data and multiple comparisons testing

In all cases, significance was tested using artificial null distributions to create probability values (p values), and control against multiple comparisons on these p values. This method used percentiles rather than a standard test (z, T, etc.) to allow uniform statistical testing to be done regardless of the shape of the data.

To generate p values for the coherence spectrum, the following process was used: An artificial null distribution was created by, prior to the quadratic de-trend, randomly circularly shifting each LFP data time course over time (uniformly distributed between one sample and the length of the signal minus one sample). This allowed inherent frequencies present in both signals to be kept, but shuffled where epochs of activity within a given frequency may have occurred in both signals. This was done 100 times and mean coherence spectra between infraslow LFP and BOLD were calculated each time. At each of the 2,000 frequency steps the 100 randomization runs were taken as a null distribution; a one-tailed p value was then calculated for the actual value using the cumulative distribution function of the null distribution. This produced 4,000 p values (2 anesthesia, 2,000 frequency steps).

To test $r_{\text{lfp-bold-template}}$ and $r_{\text{lfp-template}}$ for significance, the following process was used: Analysis described in sections *2.6* through *2.9* were repeated, except that, within each rat and anesthesia combination, which LFP recordings corresponded to which BOLD scans was randomized. This was done 10 times without replacement (derangement), producing a range of mean $r_{\text{lfp-bold-template}}$ and mean $r_{\text{lfp-template}}$ values across all tested time/frame shifts. (Only 10 randomizations were done in this case as it was more computationally intensive than others, taking over four hours for 10, while the other tests took less than four hours for 100.) For each anesthesia, these values were combined across electrodes and time/frame shifts to form null distributions of $r_{\text{lfp-bold-template}}$ and $r_{\text{lfp-template}}$. Two-tailed p values were calculated for each actual $r_{\text{lfp-bold-template}}$ and $r_{\text{lfp-template}}$ value from the cumulative distribution function of their respective null distributions.

For control against multiple comparisons, each family of p values (here defined as each figure being its own family of hypotheses) was tested using Sequential Goodness of Fit (SGoF) (Carvajal-Rodriguez et al., 2009) to find a p value threshold that allowed only 5% family-wise error rate (FWER) or less.

SGoF controls FWER in the weak sense (a large number of small p values is significant, rather than individual p values being sufficiently small) so it has the advantage that type II error rate (false negative) does not increase as the number of tests increase. In addition, it can reject p values of zero as non-significant. This is advantageous as the data randomization used here can result in p values of zero if an actual value falls outside of the generated null distribution.

3. Results

Data were used from ten Sprague-Dawley rats, under either isoflurane anesthesia (four rats) or dexmedetomidine (seven rats, one of which also had data recorded under isoflurane) using simultaneous recording of broadband (0-100Hz) LFP and single-slice fMRI BOLD imaging (Pan et al., 2010) (Supplemental figure S1).

Simultaneous recording was successful, as the artifacts due to simultaneous fMRI recording could be removed from the LFP signal and the LFP electrodes caused minimal artifacts in the EPI images (Supplemental figure S1).

3.1 BOLD-LFP coherence

Coherence is plotted in Figure 2. Significance testing using Sequential Goodness of fit (SGoF) (Carvajal-Rodriguez et al., 2009) produces a threshold of $p \leq 0.0100$. Isoflurane was statistically significant for frequencies from 0.037 to 0.159Hz. Dexmedetomidine was statistically significant for frequencies from 0.034 to 0.357Hz, from 0.358 to 0.359Hz, 0.367 to 0.368Hz and 0.369 to 0.377Hz.

The result that BOLD-LFP coherence was found to be significant for a peak in the low frequencies matches what was seen in Pan et al. (Pan et al., 2013). The "first large peak" (see *2.4*) of coherence was defined as from 0.038 to 0.184Hz under isoflurane and 0.045 to 0.304Hz under dexmedetomidine. These peaks were used as empirical filters for the respective anesthesias (Figure 2, further explanation in *2.5*). The empirical filter was compared to a traditional boxcar filter from 0.005 to 0.1Hz (Liu et al., 2010), results are shown in Table I. Standard deviation in maximum correlation value for $r_{lfp\text{-}bold}$ and time shift to maximum $r_{lfp\text{-}bold}$ are lower using the empirical filter for both anesthetics, indicative of greater error when the standard filter is used. Because it produced results with lower error but produced similar correlation values, the empirical filter was used for all further analysis.

3.2 Time-lagged BOLD-LFP correlation

Movie files (examples included in supporting information) were created for Pearson correlation between LFP and BOLD at different time shifts, referred to as $r_{lfp\text{-}bold}$. Each frame of the movie represented a time shift from BOLD 3s prior to LFP to BOLD 10s after LFP in 0.25s intervals. Table II shows the results from a qualitative visual examination of these movies. Almost all (> 97%) correlation time series showed alternation between positive and negative correlations, and over half (51.5% for isoflurane, 69.0% for dexmedetomidine) of all correlation time series showed cortical ventral-dorsal propagation . This matches the direction of propagation previously observed for QPPs in the rat cortex (Majeed et al., 2011; Majeed et al., 2009). Approximately one in ten (8.82% isoflurane, 12.0% dexmedetomidine) $r_{lfp\text{-}bold}$ patterns showed cortical dorsal-ventral propagation. For the rest of correlation time series, if there was any direction to propagation it was not readily discernible. Figure 3 illustrates $r_{lfp\text{-}bold}$ at three spatial points along the cortex; more dorsal cortical locations have peak signal at longer lag times, suggesting propagation, and the correlation alternates between high positive and high negative as the time shift increases. LFP-BOLD correlations across entire slices are shown in Figure 4 parts a and c, and are included as movie files in supplemental information.

3.3 LFP-BOLD correlation and QPP templates

QPP templates were generated for all rats and scans using the Majeed et al. algorithm (Majeed et al., 2011), a pattern-finding method that iteratively locates occurrences of a repeating QPP pattern and averages them together to create a template of the pattern. The resulting template describes a typical pattern of the spatial evolution of the 'background' BOLD signal over time; these patterns tend not to be truly periodic, but repeat several times over isolated epochs of time (hence quasi-periodic) (Majeed et al., 2011). The quasi-periodic nature of these patterns can be seen when examining their strength over time, which waxes and wanes (Supplemental figure S3). The inverse of the frequency center of mass from the empirical filters was used as the template length (11.25s for isoflurane, 6.50s for dexmedetomidine, see Figure 2 b) and templates were aligned in phase to the first template that was generated for that anesthetic. Examples of these templates are shown in Figure 4 parts b and d. The patterns of BOLD signal propagation are similar in appearance to the patterns of time-lagged BOLD-LFP correlation shown in Figure 4 a and c. Note that templates are generated using BOLD fMRI data alone, independent of electrophysiology.

To quantify the similarity between the time-lagged infraslow LFP-BOLD correlation ($r_{lfp\text{-}bold}$) and the QPP template generated by the Majeed, et al. algorithm (Majeed et al., 2011) (using the BOLD signal alone), spatial correlation of the two patterns was calculated. This spatial correlation, as a function of frame shift, was denoted $r_{lfp\text{-}bold\text{-}template}$. If it is significant, it indicates that the two patterns are spatially similar. Mean results for $r_{lfp\text{-}bold\text{-}template}$ are shown in Figure 5, individual rats are shown in Supplemental figure S2, and exact values can be found in Supplemental table SI. By multiple comparisons correction

with SGoF, p values less than or equal to 0.0160 were considered to be significant at 5%. A maximum mean value of $r_{lfp\text{-}bold\text{-}template} = 0.233$ was observed for isoflurane and $r_{lfp\text{-}bold\text{-}template} = 0.275$ for dexmedetomidine (mean across electrodes, scans, rats). The frame shift of maximum $r_{lfp\text{-}bold\text{-}template}$ was labeled as frame zero (as template phases are arbitrary). At positive and negative frame shifts, side-peaks were observed. Both the maximum mean value and its side-peaks were statistically significant when compared to a control by randomization ($p \leq 0.0160$, significant at 5% family-wise error rate (FWER) by Sequential Goodness of Fit (SGoF) (Carvajal-Rodriguez et al., 2009)). The result appeared very similar to a plot of autocorrelation versus time lag of a signal containing a single periodic process (Figure 5). Considering it to be such indicated a period of approximately 12.33s for isoflurane and 6.06s for dexmedetomidine (Equation 1). The observed period from autocorrelation was consistent with the period of the templates themselves (see *3.7*). This result demonstrated that the spatiotemporal structure of LFP and BOLD correlation (Pan et al., 2013) matches what has been seen previously in fMRI-only studies (Majeed et al., 2009) and suggests that the infraslow LFPs may contribute to a large-scale modulation of cortical excitability.

3.4 Correlation between template strength and LFPs

Changes over time in the strength of the QPP templates were also directly related to filtered LFP signals. Generation of a QPP template (from the BOLD signal alone) simultaneously produces a time course of the template's strength over time; an example is shown in Supplemental figure S3. Pearson correlation, denoted $r_{lfp\text{-}template}$, was calculated between the pre-processed and filtered LFP time series and corresponding template strength time courses at time shifts up to 20s in each direction. Mean results for $r_{lfp\text{-}template}$ are illustrated in Figure 6, individual rats are shown in Supplemental figure S4 and numerical values are listed in Supplemental table SII. Resulting correlation values were much lower than spatial correlation values ($r_{lfp\text{-}template} = 0.150$ for isoflurane, $r_{lfp\text{-}template} = 0.0635$ for dexmedetomidine, mean across electrodes, scans, rats), but remained statistically significant ($p \leq 0.0161$, significant at 5% FWER by SGoF) in every case for a large central peak and two negative side peaks, and in some cases for one or two positive side peaks. This result appeared similar to an autocorrelation series, and the results of estimating it as such are also shown on Supplemental table SII. These results provide further support for a link between low frequency LFPs and the quasi-periodic BOLD patterns.

3.5 Use of median instead of mean

The median $r_{lfp\text{--}template}$ was calculated in addition to the mean value. Results are shown in Supplemental figure S5. Every result showed significance for the largest central peak.

3.6 Test of preliminary caudate-putamen electrical recording

Calculating $r_{lfp\text{-}bold}$, using an electrode implanted in the caudate-putamen and BOLD regions of interest in the caudate-putamen, resulted in a dynamic pattern propagating from ventral to dorsal caudate-putamen, most visible in the contralateral side (Figure 7 b). Using regions of interest in interhemispheric caudate-putamen to calculate a QPP template also resulted in visible propagation of high signal from ventral to dorsal caudate-putamen (Figure 7 a). Calculation of $r_{lfp\text{-}bold\text{-}template}$, spatial correlation between the two patterns at every frame shift, did not result in an autocorrelation-like series, though it did result in several peaks of comparatively high correlation ($r_{lfp\text{-}bold\text{-}template} > 0.3$, Figure 7 c) and does resemble some individual rats' $r_{lfp\text{-}bold\text{-}template}$ (Supplemental figure S2), if not the mean.

3.7 Power spectrum of template strength versus time

Power spectra were calculated for the template strength time courses (based on correlation with the template in a sliding window). Under isoflurane a single peak was observed at approximately 0.0713 Hz or 14.0 s and under dexmedetomidine two peaks were observed approximately 0.151 Hz or 6.62s s and 0.209 Hz or 4.78 s. These frequencies are consistent with the period of the QPPs calculated from considering $r_{\text{lfp-bold-template}}$ and $r_{\text{lfp-template}}$ to be auto-correlation spectra, further strengthening the link between infraslow LFP and these templates.

4. Discussion

4.1 Summary

The present study suggests that the previously observed QPPs (Majeed et al., 2011; Majeed et al., 2009) and the low-frequency local field potentials that correlate with fMRI (Pan et al., 2013) share a common mechanism. Expanding on work by Pan et al. (Pan et al., 2013), empirical filters were constructed from the coherence between BOLD and LFP and these were used to produce lower-error correlation between the two signals (Table I). After empirically filtering both signals to infraslow frequencies, the spatiotemporal pattern of correlation between BOLD and LFP (every voxel, with multiple time shifts between the two signals) was examined. Visual inspection (Table II) showed that this pattern had the same type of propagation as the quasi-periodic patterns previously observed by Majeed et al. (Majeed et al., 2009). Examples can be seen in Figure 3, Figure 4a, Figure 4c and the included movie files in the supplemental information.

Several methods were used to statistically validate that the QPPs matched well with the infraslow LFP signal. To quantify the QPPs, an algorithm developed by Majeed et al. (Majeed et al., 2011) was used to find characteristic templates for each rat and scan (Figure 4b and Figure 4d), and these templates were registered to the first rat and scan for each anesthetic. First, spatial correlation was calculated between the spatiotemporal pattern of BOLD and LFP correlation ($r_{\text{lfp-bold}}$) and the corresponding templates. This result showed an autocorrelation-like trace (Figure 5) with an estimated period similar to the period of the template itself (Supplemental table SI vs. *3.7*). Second, regular cross-correlation was calculated between the filtered, normalized LFP signal and the time course of template strength ($r_{\text{lfp-template}}$). Correlation values in this result were smaller, but also resembled an autocorrelation spectrum (Figure 6) with an estimated period similar to the period of the template itself (Supplemental table SII vs. *3.7*). Together, these results suggest that QPPs have some basis in the underlying infraslow LFP, likely a neural or glial basis.

The central results, described in the previous paragraph, were confirmed with further tests. First, to control against possible statistical biases, calculation of $r_{\text{lfp-template}}$ was repeated with use of median instead of mean. In this case, results were similar (Supplemental figure S5) suggesting that the significant correlations observed were not an artifact of averaging correlation values. Calculation of $r_{\text{lfp-bold-template}}$ was repeated on a single rat's data where the electrode was placed in the caudate-putamen, and templates were generated from interhemispheric caudate-putamen. Results (Figure 7) were high correlation that was generally similar to the previous results from S1FL-implanted electrodes, but $r_{\text{lfp-bold-template}}$ did not resemble an autocorrelation spectrum. This is probably because the result is from a single rat and single scan only, while other results are from 4 or 7 rats and a total of 17 or 46 scans (for isoflurane or dexmedetomidine). If Supplemental figure S2 is examined, it can be seen that several individual rats have $r_{\text{lfp-bold-template}}$ similar to what was seen for the caudate-putamen. In addition, the empirical filter used to filter data strongly improved results, but was generated for S1FL and may be different for the caudate-putamen brain

regions. Nevertheless, this result suggests that, with more rats and a properly created empirical filter, the results of this study may translate to other brain regions.

Overall, the results suggest that the infraslow LFP and BOLD correlates that appeared as a spatiotemporal pattern in Pan et al. (Pan et al., 2013) reflect a QPP as previously observed by Majeed et al. in fMRI alone (Majeed et al., 2009). While the present results are limited to a single fMRI slice and two electrical recording sites, the implication is that the QPPs observed in the spontaneous BOLD signal (Majeed et al., 2011; Majeed et al., 2009) reflect a quasi-periodic, slow wave of electrical potential changes that make up a statistically significant portion of the infraslow LFP. Another study by Majeed et al. demonstrated that QPPs extend throughout the brain and are present in humans as well (Majeed et al., 2011). This, combined with the results of the present study, suggest that studying QPPs may be useful in our efforts to understand the spontaneous fMRI signal in humans.

4.2 Possible common mechanisms for QPPs and LFP-BOLD correlations

As LFPs were recorded only from a single point in each hemisphere, we cannot be certain that every point along the QPP's path seen in fMRI is reflecting a corresponding infraslow electrical potential; it is thus possible that the appearance of propagation in both the BOLD-based QPP templates and the infraslow LFP-BOLD correlation maps is vascular in origin. Large veins point downward into the rat cortex (Lin et al., 2009), and arteries point upward, dorsal-medially. A change in blood flow can create a change in arterial diameter; the time scale of this change is on the order of seconds for distances on the order of millimeters (Porret et al., 1998). The correlation with field potentials could be synchrony between this highly coordinated vasomotion and large scale slow fluctuations in the brain, such as occasional global sleep waves (Steriade et al., 1993a; Steriade et al., 1993b, c) or a hypothetical global neural electrical signal (Scholvinck et al., 2010).

Neural and glial mechanisms could also allow for slow, propagating changes in the electrical field. Thalamocortical neurons may initiate slow wave activity through calcium ions (Hughes et al., 2002) and this neural activation may increase astrocytic calcium concentrations, inducing a wave that can propagate to other astrocytes on a scale of tens of seconds (Kuga et al., 2011). The interplay between the blood vessel directionality described above and changing intracellular calcium concentrations that cause local vessel dilation (Girouard et al., 2010; Iadecola and Nedergaard, 2007), or astrocytic dynamics (Kuga et al., 2011) may tentatively explain the direction of the dynamics observed here.

To test which of these hypotheses is more likely, the infraslow LFP at multiple sites along the pattern of propagation would need to be recorded. However in either case, the dynamics are likely linked to information processing as they would be relating to either a global signal with a neural basis (Scholvinck et al., 2010) or localized dynamics such as those previously linked to behavior in fMRI (Eichele et al., 2008; Thompson et al., 2012).

4.3 Implications for dynamic analysis of functional connectivity

While fMRI-based functional connectivity is typically calculated for an entire resting state scan (5-10 minutes), interest is growing in identifying changes that occur on much shorter time scales (12-100 seconds) (Allen et al., 2012; Chang and Glover, 2010; Chang et al., 2013; Handwerker et al., 2012; Hutchison et al., 2013; Hutchison et al., 2012; Keilholz et al., 2013; Kiviniemi et al., 2011; Sakoglu et al., 2010; Thompson et al., 2012; Thompson et al., 2013). However, preliminary attempts using correlation calculated in sliding time windows have had mixed results as the signal dynamics in some cases appear indistinguishable from randomly-matched or artificial data (Handwerker et al., 2012; Keilholz et al., 2013). Early evidence has suggested that at least some of the measured

changes in connectivity over time may have a neural or glial basis in the higher-frequency bands; both in large-scale electroencephalogram (EEG) bands (Chang et al., 2013) and electrical activity local to an electrode (Thompson et al., 2013).

The relationship observed between electrical potential changes in the brain and fMRI in the present study may represent a different aspect of neural or glial activity than is reflected by sliding window correlation. The strongest relationship seen between sliding window functional connectivity and local electrical activity was in the beta and gamma bands, 25 to 100Hz (Thompson et al., 2013). The amplitudes of local LFP and BOLD signals are also related in these frequencies; however when examined at multiple time shifts they do not show a spatiotemporal structure as was observed with infraslow LFP in the present study and by Pan et al. (Pan et al., 2013). Instead, they appear to only be highly correlated local to the electrode's position and in the contralateral homologous position, at a time delay mimicking the hemodynamic response seen in previous studies of activation (Pan et al., 2011). While both assume a linear relationship between different brain areas, QPPs and sliding window correlation are otherwise fundamentally different ways of analyzing the time-varying components of functional connectivity. Based on the differences between this study and previous work investigating the neural basis of sliding window correlation (Chang et al., 2013; Thompson et al., 2013), it is very possible that QPPs and sliding window correlation are reflecting different aspects of the underlying neural activity. Specifically, QPP-based methods are likely better reflecting at infraslow phases or amplitudes while sliding window correlation methods are likely better at reflecting power changes in higher frequencies. Conversely, it is still possible that these two different methods are representing the same underlying neural or glial sources. Earlier work from the present study's authors demonstrated a consistent link between correlation in sliding windows and behavior by focusing on the networks where QPPs have been observed in humans (Thompson et al., 2012).

The results of this study also highlight some of the pitfalls involved in standard functional connectivity analysis techniques. No correlation is typically observed between lateral and medial cortical areas in the rat (Pawela et al., 2009; Williams et al., 2010; Zhao et al., 2008), but the present study suggests this may be due to a time lag resulting from a propagating dynamic. Perhaps the entire somatomotor cortex could be considered a network, with sub-networks connecting interhemispherically homologous areas.

Based on that observation from the rat cortex, it is interesting to speculate, given the pattern of QPPs in humans (Majeed et al., 2011), that the default and attention networks are also part of a larger organization. In humans, the fMRI signal in the default mode network appears anti-correlated to the signal from attention areas (Fox et al., 2005; Fransson, 2005), to the point where a “task positive” network can be defined from this anti-correlation. Interestingly, greater anti-correlation is related to faster or more accurate performance on a several tasks (Eichele et al., 2008; Kelly et al., 2008; Prado and Weissman, 2011; Thompson et al., 2012; Weissman et al., 2006). QPP strength was observed in the present study to correlate significantly (if weakly) with infraslow LFP (Figure 6). This would imply both positive-sloping and negative-sloping deflections of QPP strength may be linked to LFP deflections, suggesting that both the positive and negative alternations in the QPPs themselves may be relevant. These positive and negative alternations were seen under both anesthetics, implying they were not an anesthetic-specific effect (Table II). If, in humans, part of the default mode and task positive networks arises from the spatiotemporal structure of a QPP, then a greater QPP strength would result in more anti-correlation being measured, and thus better performance. While it is purely speculative, it is possible that some pattern of infraslow LFP fluctuations is actually a single mechanism behind these two “networks.” This may explain why some groups have seen a relationship between infraslow EEG and

performance as well (Demanuele et al., 2010; Monto et al., 2008; Trimmel et al., 1990; Trimmel et al., 2001)

4.4 Use of anesthesia

An anesthetized rat model is used in the present study because it allows for invasive recording of infraslow electrical potentials simultaneously with fMRI of a single image slice (Pan et al., 2010; Pan et al., 2013). Therefore the infraslow potentials can be compared to part of the brain. While the amount of the brain imaged is limited in this model, it still allows a greater extent of visualization of activity than individual electrical recording sites. In addition, the QPPs to be examined were first detected in an anesthetized rat model, and in this model the QPP can be observed in a single image slice (Majeed et al., 2009).

This study uses two different anesthetic agents on rats during data recording; isoflurane and dexmedetomidine. These anesthesias were chosen because they are commonly used in functional connectivity fMRI experiments in rodents, because of their ease of use, because functional networks can be observed in them (Liu et al., 2012; Pawela et al., 2009), and because such networks are hypothetically homologous to the functional networks seen in awake humans.

This study primarily made comparisons within anesthesia groups, between different measurement methods (infraslow LFP, and QPPs from fMRI), so that the two anesthesias were used primarily to act as a control against one another, rather than used to compare between anesthetic conditions. Dexmedetomidine and isoflurane are different both in terms of their effects on the vasculature that creates the fMRI signal and in terms of their effect on neural activity that suppresses awake behavior (see Appendix A). The primary purpose of this study was to determine if the fMRI correlates of infraslow LFP and the QPPs share a common mechanism. Therefore, most comparisons were done within each anesthesia without comparison to the other anesthesia. As similar significant results were found within each anesthesia, it was generally concluded that anesthesia-specific effects are unlikely to be causing the significant results seen in this study. However, differences between dexmedetomidine and isoflurane exist which can be seen when comparing results across the two anesthesias in this study.

If results are compared across anesthesia groups, it suggests that isoflurane has a lower frequency relationship to the BOLD and thus has slower QPPs observed than dexmedetomidine. Figure 2 shows that the coherence between fMRI and LFP extends into higher frequencies for dexmedetomidine. Isoflurane had a longer lag time to peak correlation between LFP and fMRI data from the same location (Table I, first row, second and fifth columns). The time scale on Figure 4 and the supplemental movie files show that the QPPs appear to propagate more slowly under isoflurane than under dexmedetomidine. As would be expected from slower QPPs, the correlation between spatiotemporal patterns (Figure 5) and QPP strength and the LFP itself (Figure 6) plots for isoflurane have greater distance between peaks. This result matches what was previously observed by Pan et al. (Pan et al., 2013) and expands it to include QPP which were not previously considered.

Pan et al. suggested two possibilities for the source of the greater lag under isoflurane. In the first possibility, the difference is due to dexmedetomidine and isoflurane affecting the vascular tone in very different manners (see Appendix A and (Ohata et al., 1999)). The observed increase in the periods of QPPs would thus suggest that QPPs may be propagating through vasomotion. In the second possibility, the infraslow potential changes observed are due to astrocytes triggering UP states (Poskanzer and Yuste, 2011), and the greater delay under isoflurane is due to astrocytic calcium release being delayed by a few seconds relative to neural firing (Schummers et al., 2008) with dexmedetomidine allowing astrocytes to

release calcium concurrent with neural activity. In this case, the increase in periods of QPPs would indicate that their propagation requires astrocytic calcium release at several points to propagate, which is delayed at each point.

Understanding the physiological basis of the change in the time shift (between LFP and fMRI) under different anesthetic conditions may help explain the underlying mechanism behind QPPs. Future work that takes direct measurement of blood vessel size and measures intracellular calcium may help answer these questions.

4.5 Other limitations of the study

The QPPs observed in this study are unlikely to be artifactual in origin. Previous work using fast imaging (10Hz) has shown that these dynamics are not related to aliasing of cardiac or respiratory frequency components, nor are they related to scanner noise as they do not occur in euthanatized rats under the same setup (Majeed et al., 2009) and occur in both humans and rats, under different scan parameters for both species (Majeed et al., 2011). It is unlikely that they are due to local differences in signal to noise ratio because they propagate in both directions, primarily in the direction towards the electrode, the opposite of the direction proposed for this artifact by Logothetis et al. (Logothetis et al., 2009). Animals were imaged in the dark, under anesthesia, and typical forepaw stimulation equipment was not attached, so stimulus artifacts can be excluded.

It also must be considered that the present study used regression of the mean signal from all brain voxels to reduce the noise due to non-localized scanner artifacts (Fox et al., 2005). This was required to complete the goal of this study as previous work both with infraslow potentials (Pan et al., 2013) and with QPPs (Majeed et al., 2011; Majeed et al., 2009) performed this regression, and this study combined those studies. In addition, in the anesthetized rat model, failure to regress this “global signal” can complicate comparison between different anesthesia levels (Liu et al., 2012). However, global signal regression has the potential to introduce artifactual anti-correlation (Gavrilescu et al., 2002) even if it may not do so in practice (Fox et al., 2009). Further work is needed to determine if the negative correlations observed here actually represent an antagonistic relationship, or represent low signal relative to some form of global electrical signal (Scholvinck et al., 2010).

In addition, to facilitate fast BOLD imaging with electrodes in the rat's brain, and to follow the previous work that forms the basis of this study (Majeed et al., 2009; Pan et al., 2011; Pan et al., 2013), only a single slice was recorded. This makes comparison to other work difficult, as previous work has shown that QPPs extend throughout a rat's brain (Majeed et al., 2011) yet we cannot observe the full extent of the LFP and fMRI correlation to see if it is equally related in other parts of the brain. Based on the results here being reproducible across different rats (see Supplemental figure S2, Supplemental figure S4) and the previously observed presence of QPPs across the whole brain in humans (Majeed et al., 2011) it seems likely that these results would translate to other brain regions. Improved simultaneous imaging methods, improved infraslow LFP recording capabilities and faster BOLD imaging methods may allow future work to improve upon these results.

4.6 Conclusion

The location of QPPs in this model closely match known functional networks in the rodent (Majeed et al., 2009; Williams et al., 2010). QPPs have also been demonstrated during the resting state in human subjects (Majeed et al., 2011), and they appear to also exist in well-studied known networks; the default mode and task positive networks (Majeed et al., 2011). These networks have been linked to numerous diseases and behavioral variations: fairly early they were linked to Alzheimer's disease (Greicius et al., 2004; Rombouts et al., 2005),

but much recent interest has been in their connection to the ability to maintain attention (Eichele et al., 2008; Kelly et al., 2008; Prado and Weissman, 2011; Thompson et al., 2012; Weissman et al., 2006). Interestingly, a few groups have also found a link between attention or reaction time and infraslow EEG potentials (Helps et al., 2008; Helps et al., 2010; Trimmel et al., 1990; Trimmel et al., 2001). Future work could explore this potential from either direction, to measure infraslow EEG's spatiotemporal patterns and compare it to QPP from simultaneous or separately recorded fMRI studies, or to compare QPP to behavior and see if its relationship is similar to infraslow EEG.

Because QPPs have also been observed in awake human subjects, the results of the current study are interesting as they imply a possible electrical basis for observed spatiotemporal patterns seen in fMRI in human subjects as well (Grigg and Grady, 2010; Liu and Duyn, 2013; Majeed et al., 2011). The neural electrical basis of resting state functional connectivity is still poorly understood, despite its connection to numerous diseases and behaviors. QPPs in human subjects also appear to exist in the default mode network (Majeed et al., 2011), whose dynamic properties have been the subject of increasing scrutiny (Allen et al., 2012; Chang and Glover, 2010; Hutchison et al., 2013; Hutchison et al., 2012; Liu and Duyn, 2013), linked to schizophrenia (Sakoglu et al., 2010) and behavior (Thompson et al., 2012). While more work with QPPs in needed in human subjects, the implications of this study are promising for better understanding the neural basis of dynamics in the default mode network.

If the hypothesis that functional connectivity emerges from a spatiotemporal structure of brain activity is true, then it is necessary to understand the neural or glial basis of this structure. The present study has taken one of the first steps in this direction.

$$\left[\left(\mathrm{PP_L}+\mathrm{PP_R}\right)-\left(\mathrm{NP_L}+\mathrm{NP_R}\right)\right]/4 \quad \text{Equation 1}$$

Supplementary Material

Refer to Web version on PubMed Central for supplementary material.

Acknowledgments

The authors would like to thank Josh Grooms, Alessio Medda, Jeremy Edgerton, Collin Lobb, Mac Merritt and Martha Willis for their valuable help and suggestions. Funding sources: NIH, 1R21NS072810-01A1 and 1R21NS057718-01; Scholarly Inquiry and Research at Emory (SIRE) Fellowship program at Emory University.

Appendix A

Anesthesia mechanisms and physiological effects

Isoflurane is a gaseous anesthesia with a long history of use in both human patients and nonhuman animal research. Its primary mechanism of anesthesia is not fully understood, but is thought to be suppression of neural activity through inhibition of GABA and glutamate receptors at thalamocortical connections (Alkire et al., 2000), resulting in a burst pattern in cortical LFP where greater anesthetic dose results in greater burst suppression (Pan et al., 2011; Vincent et al., 2007). Large-scale vascular dilation has been long observed under isoflurane (Reiz et al., 1983) which has been suggested to be due to blockage of adenosine triphosphate sensitive potassium (KATP) channels in smooth muscle (Cason et al., 1994). This vascular dilation likely influences the hemodynamic response seen in fMRI (Liu et al., 2010; Pan et al., 2011). The vasodilation (Lennon and Murray, 1995; Schwinn et al., 1990) mechanisms of isoflurane are believed to be independent of alpha adrenergic systems, and

the authors were unable to find discussion of adrenergic systems in work describing isoflurane's mechanisms of cortical suppression (Alkire et al., 2000; Ries and Puil, 1999). While adrenergic systems may play a role in analgesic properties of isoflurane (Kingery et al., 2002), to the best of our knowledge these have only been implicated outside the brain.

Medetomidine and its enantiomer dexmedetomidine is an anesthesia that has recently been gaining popularity for small animal fMRI studies as it can be administered subcutaneously to freely breathing animals (Pawela et al., 2009). Medetomidine binds in a highly specific fashion to alpha-2 adrenoreceptors. Blockage of these receptors in the central nervous system prevents release of norepinephrine, and as norepinephrine is required for awake behaviors, sedation occurs (Sinclair, 2003). As medetomidine requires a sedative effect to maintain anesthesia, its effect is not as strong as isoflurane; stress may prevent sedation, and sedated animals may awaken if disturbed by a loud noise, pain or physical movement (Sinclair, 2003). Opposite to isoflurane, medetomidine has been shown to induce vasoconstriction in the cerebral vasculature, which is likely due to the direct effect of alpha-2 receptors within cerebral vasculature (Ganjoo et al., 1998).

As the two anesthetic agents, first, have hypothetically non-overlapping mechanisms for both their anesthetic and vascular active properties, second, have different effects on vasculature, and third, have vastly different strength, we suggest that in the present study each one acts as a control for many possible anesthetic effects against the other. In fact, it has been suggested dexmedetomidine to reverse the vascular effects of isoflurane (Zornow et al., 1990) and isoflurane to reverse epileptiform effects of dexmedetomidine overdose (Fukuda et al., 2012). While comparing results under both anesthesias cannot control against the anesthetic state in general, commonalities observed between them are unlikely to be due to the particularities of any one anesthesia.

Appendix B

Parameters used in algorithm from Majeed et al. 2011

In this study, an algorithm for finding templates and strength over time from quasi-periodic patterns (QPP) was used that has been previously described in detail in Majeed et al. (Majeed et al., 2011). The algorithm itself was used without modification, however, the specific parameters were unique to this study and are as follows: The template length was set to the frequency location of the center of mass of the empirically derived filter; this was intended to force the template to be only one period of the QPP. The start point of the template was held constant at 250 seconds, as, in rats, the start point is unlikely to affect the resulting QPP in any sense other than its phase (Majeed et al., 2011; Majeed et al., 2009). The region of interest was set to a combination of both the left and right S1FL ROIs. Thresholds were set arbitrarily low to ensure convergence; the first threshold was 0.001 (1/100th of default) for 3 iterations (default) and the second threshold was 0.002 (1/100th of default) for a up to 10,000 (500 times default) iterations.

As templates are likely to be consistent but of different phases (Majeed et al., 2011; Majeed et al., 2009), templates were set to the same phase on a per-anesthesia basis in the following manner: The template was circularly shifted in time (e.g. a shift of 1 would remove one frame from the end and place it at the beginning) for each possible frame shift (from zero to the length of the template) and normalized spatial correlation was calculated in MATLAB using the normxcorr2 function between the circularly shifted template and the template generated for the first rat and scan for that anesthesia (the first rat and scan was taken arbitrarily as templates are likely to be consistent except for phase). The central 25% (spatial shifts of up to 25%) of correlation values were summed. The circular frame shift where the

sum correlation was at a maximum was used for further analysis. The amount of this shift, in seconds, was also applied as a non-circular, zero-replacing shift (e.g. a shift of 1 would remove one point from the end and add a zero to the beginning) to the template strength versus time. These alignments are shown in the center of Figure 1.

Abbreviations

fMRI	functional magnetic resonance imaging
BOLD	blood oxygen level dependent
QPP	quasi-periodic pattern
LFP	local field potentials
EEG	electroencephalography
S1FL	primary somatosensory cortex of the forelimb region
EPI	echo-planar imaging
SGoF	sequential goodness of fit
FWER	family-wise error rate
PPL	positive peak on left
PPR	positive peak on right
NPL	negative peak on left
NPR	negative peak on right

References

Agranovskii AV, Berg O, Evreinov GE. [Experimental evaluation of materials for electrodes in transcutaneous recording of bioelectric signals]. Med Tekh. 1998:23–27. [PubMed: 9560814]

Albert NB, Robertson EM, Miall RC. The resting human brain and motor learning. Curr Biol. 2009; 19:1023–1027. [PubMed: 19427210]

Alkire MT, Haier RJ, Fallon JH. Toward a unified theory of narcosis: brain imaging evidence for a thalamocortical switch as the neurophysiologic basis of anesthetic-induced unconsciousness. Conscious Cogn. 2000; 9:370–386. [PubMed: 10993665]

Allen EA, Damaraju E, Plis SM, Erhardt EB, Eichele T, Calhoun VD. Tracking Whole-Brain Connectivity Dynamics in the Resting State. Cereb Cortex. 2012

Allen PJ, Josephs O, Turner R. A method for removing imaging artifact from continuous EEG recorded during functional MRI. Neuroimage. 2000; 12:230–239. [PubMed: 10913328]

Birbaumer N, Elbert T, Canavan AG, Rockstroh B. Slow potentials of the cerebral cortex and behavior. Physiol Rev. 1990; 70:1–41. [PubMed: 2404287]

Biswal B, Yetkin FZ, Haughton VM, Hyde JS. Functional connectivity in the motor cortex of resting human brain using echo-planar MRI. Magn Reson Med. 1995; 34:537–541. [PubMed: 8524021]

Boly M, Balteau E, Schnakers C, Degueldre C, Moonen G, Luxen A, Phillips C, Peigneux P, Maquet P, Laureys S. Baseline brain activity fluctuations predict somatosensory perception in humans. Proc Natl Acad Sci U S A. 2007; 104:12187–12192. [PubMed: 17616583]

Carvajal-Rodriguez A, de Una-Alvarez J, Rolan-Alvarez E. A new multitest correction (SGoF) that increases its statistical power when increasing the number of tests. BMC Bioinformatics. 2009; 10:209. [PubMed: 19586526]

Cason BA, Shubayev I, Hickey RF. Blockade of adenosine triphosphate-sensitive potassium channels eliminates isoflurane-induced coronary artery vasodilation. Anesthesiology. 1994; 81:1245–1255. discussion 1227A-1228A. [PubMed: 7978484]

Chang C, Glover GH. Time-frequency dynamics of resting-state brain connectivity measured with fMRI. Neuroimage. 2010; 50:81–98. [PubMed: 20006716]

Chang C, Liu Z, Chen MC, Liu X, Duyn JH. EEG correlates of time-varying BOLD functional connectivity. Neuroimage. 2013; 72:227–236. [PubMed: 23376790]

Cordes D, Haughton VM, Arfanakis K, Wendt GJ, Turski PA, Moritz CH, Quigley MA, Meyerand ME. Mapping functionally related regions of brain with functional connectivity MR imaging. AJNR Am J Neuroradiol. 2000; 21:1636–1644. [PubMed: 11039342]

Deco G, Jirsa VK, McIntosh AR. Emerging concepts for the dynamical organization of resting-state activity in the brain. Nat Rev Neurosci. 2011; 12:43–56. [PubMed: 21170073]

Demanuele C, Sonuga-Barke EJ, James CJ. Slow neuronal oscillations in the resting brain vs task execution: A BSS investigation of EEG recordings. Conf Proc IEEE Eng Med Biol Soc. 2010; 2010:1638–1641. [PubMed: 21096137]

Drew PJ, Duyn JH, Golanov E, Kleinfeld D. Finding coherence in spontaneous oscillations. Nat Neurosci. 2008; 11:991–993. [PubMed: 18725901]

Drummond SP, Bischoff-Grethe A, Dinges DF, Ayalon L, Mednick SC, Meloy MJ. The neural basis of the psychomotor vigilance task. Sleep. 2005; 28:1059–1068. [PubMed: 16268374]

Eichele T, Debener S, Calhoun VD, Specht K, Engel AK, Hugdahl K, von Cramon DY, Ullsperger M. Prediction of human errors by maladaptive changes in event-related brain networks. Proc Natl Acad Sci U S A. 2008; 105:6173–6178. [PubMed: 18427123]

Fox MD, Snyder AZ, Vincent JL, Corbetta M, Van Essen DC, Raichle M. The human brain is intrinsically organized into dynamic, anticorrelated functional networks. Proc Natl Acad Sci U S A. 2005; 102:9673–9678. [PubMed: 15976020]

Fox MD, Zhang DY, Snyder AZ, Raichle ME. The Global Signal and Observed Anticorrelated Resting State Brain Networks. Journal of Neurophysiology. 2009; 101:3270–3283. [PubMed: 19339462]

Fransson P. Spontaneous low-frequency BOLD signal fluctuations: an fMRI investigation of the resting-state default mode of brain function hypothesis. Hum Brain Mapp. 2005; 26:15–29. [PubMed: 15852468]

Fukuda M, Vazquez AL, Zong X, Kim SG. Effects of the alpha(2) -adrenergic receptor agonist dexmedetomidine on neural, vascular and BOLD fMRI responses in the somatosensory cortex. European Journal of Neuroscience. 2012

Ganjoo P, Farber NE, Hudetz A, Smith JJ, Samso E, Kampine JP, Schmeling WT. In vivo effects of dexmedetomidine on laser-Doppler flow and pial arteriolar diameter. Anesthesiology. 1998; 88:429–439. [PubMed: 9477064]

Garrity AG, Pearlson GD, McKiernan K, Lloyd D, Kiehl KA, Calhoun VD. Aberrant “default mode” functional connectivity in schizophrenia. Am J Psychiatry. 2007; 164:450–457. [PubMed: 17329470]

Gavrilescu M, Shaw ME, Stuart GW, Eckersley P, Svalbe ID, Egan GF. Simulation of the effects of global normalization procedures in functional MRI. Neuroimage. 2002; 17:532–542. [PubMed: 12377132]

Geddes LA, Roeder R. Measurement of the Direct-Current .Faradic. Resistance of the Electrode-Electrolyte Interface for Commonly Used Electrode Materials. Annals of Biomedical Engineering. 2001; 29:181–186. [PubMed: 11284673]

Geddes LA, Roeder R. Criteria for the Selection of Materials for Implanted Electrodes. Annals of Biomedical Engineering. 2003; 31:879–890. [PubMed: 12971619]

Girouard H, Bonev AD, Hannah RM, Meredith A, Aldrich RW, Nelson MT. Astrocytic endfoot Ca2+ and BK channels determine both arteriolar dilation and constriction. Proc Natl Acad Sci U S A. 2010; 107:3811–3816. [PubMed: 20133576]

Greicius MD, Srivastava G, Reiss AL, Menon V. Default-mode network activity distinguishes Alzheimer's disease from healthy aging: evidence from functional MRI. Proc Natl Acad Sci U S A. 2004; 101:4637–4642. [PubMed: 15070770]

Grigg O, Grady CL. Task-related effects on the temporal and spatial dynamics of resting-state functional connectivity in the default network. PLoS One. 2010; 5:e13311. [PubMed: 20967203]

Hampson M, Driesen NR, Skudlarski P, Gore JC, Constable RT. Brain connectivity related to working memory performance. J Neurosci. 2006; 26:13338–13343. [PubMed: 17182784]

Handwerker DA, Roopchansingh V, Gonzalez-Castillo J, Bandettini PA. Periodic changes in fMRI connectivity. Neuroimage. 2012; 63:1712–1719. [PubMed: 22796990]

He BJ, Snyder AZ, Zempel JM, Smyth MD, Raichle ME. Electrophysiological correlates of the brain's intrinsic large-scale functional architecture. Proc Natl Acad Sci U S A. 2008; 105:16039–16044. [PubMed: 18843113]

Helps S, James C, Debener S, Karl A, Sonuga-Barke EJ. Very low frequency EEG oscillations and the resting brain in young adults: a preliminary study of localisation, stability and association with symptoms of inattention. J Neural Transm. 2008; 115:279–285. [PubMed: 17994187]

Helps SK, Broyd SJ, James CJ, Karl A, Chen W, Sonuga-Barke EJ. Altered spontaneous low frequency brain activity in attention deficit/hyperactivity disorder. Brain Res. 2010; 1322:134–143. [PubMed: 20117101]

Honey CJ, Kotter R, Breakspear M, Sporns O. Network structure of cerebral cortex shapes functional connectivity on multiple time scales. Proc Natl Acad Sci U S A. 2007; 104:10240–10245. [PubMed: 17548818]

Hughes SW, Cope DW, Blethyn KL, Crunelli V. Cellular mechanisms of the slow (<1 Hz) oscillation in thalamocortical neurons in vitro. Neuron. 2002; 33:947–958. [PubMed: 11906700]

Hutchison RM, Womelsdorf T, Allen EA, Bandettini PA, Calhoun VD, Corbetta M, Della Penna S, Duyn J, Glover G, Gonzalez-Castillo J, Handwerker DA, Keilholz S, Kiviniemi V, Leopold DA, de Pasquale F, Sporns O, Walter M, Chang C. Dynamic functional connectivity: Promises, issues, and interpretations. Neuroimage. 2013; 80:360–378. [PubMed: 23707587]

Hutchison RM, Womelsdorf T, Gati JS, Everling S, Menon RS. Resting-state networks show dynamic functional connectivity in awake humans and anesthetized macaques. Hum Brain Mapp. 2012

Iadecola C, Nedergaard M. Glial regulation of the cerebral microvasculature. Nat Neurosci. 2007; 10:1369–1376. [PubMed: 17965657]

Jones TB, Bandettini PA, Kenworthy L, Case LK, Milleville SC, Martin A, Birn RM. Sources of group differences in functional connectivity: an investigation applied to autism spectrum disorder. Neuroimage. 2010; 49:401–414. [PubMed: 19646533]

Keilholz S, Magnuson ME, Pan WJ, Willis M, Thompson G. Dynamic Properties of Functional Connectivity in the Rodent. Brain Connect. 2013; 3:31–40. [PubMed: 23106103]

Kelly AM, Uddin LQ, Biswal BB, Castellanos FX, Milham MP. Competition between functional brain networks mediates behavioral variability. Neuroimage. 2008; 39:527–537. [PubMed: 17919929]

Khader P, Schicke T, Roder B, Rosler F. On the relationship between slow cortical potentials and BOLD signal changes in humans. Int J Psychophysiol. 2008; 67:252–261. [PubMed: 17669531]

Kingery WS, Agashe GS, Guo TZ, Sawamura S, Davies MF, Clark JD, Kobilka BK, Maze M. Isoflurane and nociception: spinal alpha2A adrenoceptors mediate antinociception while supraspinal alpha1 adrenoceptors mediate pronociception. Anesthesiology. 2002; 96:367–374. [PubMed: 11818770]

Kiviniemi V, Vire T, Remes J, Elseoud AA, Starck T, Tervonen O, Nikkinen J. A sliding time-window ICA reveals spatial variability of the default mode network in time. Brain Connect. 2011; 1:339–347. [PubMed: 22432423]

Kuga N, Sasaki T, Takahara Y, Matsuki N, Ikegaya Y. Large-scale calcium waves traveling through astrocytic networks in vivo. J Neurosci. 2011; 31:2607–2614. [PubMed: 21325528]

Lennon PF, Murray PA. Isoflurane and the pulmonary vascular pressure-flow relation at baseline and during sympathetic alpha- and beta-adrenoreceptor activation in chronically instrumented dogs. Anesthesiology. 1995; 82:723–733. [PubMed: 7879940]

Lin CY, Lin MH, Cheung WM, Lin TN, Chen JH, Chang C. In vivo cerebromicrovasculatural visualization using 3D DeltaR2-based microscopy of magnetic resonance angiography (3DDeltaR2-mMRA). Neuroimage. 2009; 45:824–831. [PubMed: 19154792]

Liu X, Duyn JH. Time-varying functional network information extracted from brief instances of spontaneous brain activity. Proc Natl Acad Sci U S A. 2013; 110:4392–4397. [PubMed: 23440216]

Liu X, Zhu XH, Zhang Y, Chen W. Neural Origin of Spontaneous Hemodynamic Fluctuations in Rats under Burst-Suppression Anesthesia Condition. Cereb Cortex. 2010; 21:374–384. [PubMed: 20530220]

Liu X, Zhu XH, Zhang Y, Chen W. The Change of Functional Connectivity Specificity in Rats Under Various Anesthesia Levels and its Neural Origin. Brain Topogr. 2012; 26:363–377. [PubMed: 23208517]

Logothetis NK, Murayama Y, Augath M, Steffen T, Werner J, Oeltermann A. How not to study spontaneous activity. Neuroimage. 2009; 45:1080–1089. [PubMed: 19344685]

Logothetis NK, Pauls J, Augath M, Trinath T, Oeltermann A. Neurophysiological investigation of the basis of the fMRI signal. Nature. 2001; 412:150–157. [PubMed: 11449264]

Lu H, Zuo Y, Gu H, Waltz JA, Zhan W, Scholl CA, Rea W, Yang Y, Stein EA. Synchronized delta oscillations correlate with the resting-state functional MRI signal. Proc Natl Acad Sci U S A. 2007; 104:18265–18269. [PubMed: 17991778]

Magnuson M, Majeed W, Keilholz SD. Functional connectivity in blood oxygenation level-dependent and cerebral blood volume-weighted resting state functional magnetic resonance imaging in the rat brain. J Magn Reson Imaging. 2010; 32:584–592. [PubMed: 20815055]

Majeed W, Magnuson M, Hasenkamp W, Schwarb H, Schumacher EH, Barsalou L, Keilholz SD. Spatiotemporal dynamics of low frequency BOLD fluctuations in rats and humans. Neuroimage. 2011; 54:1140–1150. [PubMed: 20728554]

Majeed W, Magnuson M, Keilholz SD. Spatiotemporal dynamics of low frequency fluctuations in BOLD fMRI of the rat. J Magn Reson Imaging. 2009; 30:384–393. [PubMed: 19629982]

Monto S, Palva S, Voipio J, Palva JM. Very slow EEG fluctuations predict the dynamics of stimulus detection and oscillation amplitudes in humans. J Neurosci. 2008; 28:8268–8272. [PubMed: 18701689]

Ohata H, Iida H, Dohi S, Watanabe Y. Intravenous dexmedetomidine inhibits cerebrovascular dilation induced by isoflurane and sevoflurane in dogs. Anesth Analg. 1999; 89:370–377. [PubMed: 10439750]

Pan WJ, Thompson G, Magnuson M, Majeed W, Jaeger D, Keilholz S. Simultaneous FMRI and electrophysiology in the rodent brain. J Vis Exp. 2010:e1901.

Pan WJ, Thompson G, Magnuson M, Majeed W, Jaeger D, Keilholz S. Broadband local field potentials correlate with spontaneous fluctuations in functional magnetic resonance imaging signals in the rat somatosensory cortex under isoflurane anesthesia. Brain Connect. 2011; 1:119–131. [PubMed: 22433008]

Pan WJ, Thompson GJ, Magnuson ME, Jaeger D, Keilholz S. Infraslow LFP correlates to resting-state fMRI BOLD signals. Neuroimage. 2013; 74C:288–297. [PubMed: 23481462]

Pawela CP, Biswal BB, Hudetz AG, Schulte ML, Li R, Jones SR, Cho YR, Matloub HS, Hyde JS. A protocol for use of medetomidine anesthesia in rats for extended studies using task-induced BOLD contrast and resting-state functional connectivity. Neuroimage. 2009; 46:1137–1147. [PubMed: 19285560]

Paxinos, G.; Watson, C. The rat brain in stereotaxic coordinates. 5th ed.. Elsevier Academic Press; Amsterdam ; Boston: 2005.

Porret CA, Stergiopulos N, Meister JJ. Flow-driven diameter response in rat femoral arteries perfused in vitro. Ann Biomed Eng. 1998; 26:526–533. [PubMed: 9662145]

Poskanzer KE, Yuste R. Astrocytic regulation of cortical UP states. Proceedings of the National Academy of Sciences of the United States of America. 2011; 108:18453–18458. [PubMed: 22027012]

Prado J, Carp J, Weissman DH. Variations of response time in a selective attention task are linked to variations of functional connectivity in the attentional network. Neuroimage. 2011; 54:541–549. [PubMed: 20728549]

Prado J, Weissman DH. Heightened interactions between a key default-mode region and a key task-positive region are linked to suboptimal current performance but to enhanced future performance. Neuroimage. 2011; 56:2276–2282. [PubMed: 21440073]

Raichle ME, MacLeod AM, Snyder AZ, Powers WJ, Gusnard DA, Shulman GL. A default mode of brain function. Proc Natl Acad Sci U S A. 2001; 98:676–682. [PubMed: 11209064]

Reiz S, Balfors E, Sorensen MB, Ariola S Jr. Friedman A, Truedsson H. Isoflurane--a powerful coronary vasodilator in patients with coronary artery disease. Anesthesiology. 1983; 59:91–97. [PubMed: 6869900]

Ries CR, Puil E. Mechanism of anesthesia revealed by shunting actions of isoflurane on thalamocortical neurons. J Neurophysiol. 1999; 81:1795–1801. [PubMed: 10200213]

Rombouts SA, Barkhof F, Goekoop R, Stam CJ, Scheltens P. Altered resting state networks in mild cognitive impairment and mild Alzheimer's disease: an fMRI study. Hum Brain Mapp. 2005; 26:231–239. [PubMed: 15954139]

Sakoglu U, Pearlson GD, Kiehl KA, Wang YM, Michael AM, Calhoun VD. A method for evaluating dynamic functional network connectivity and task-modulation: application to schizophrenia. Magma. 2010; 23:351–366. [PubMed: 20162320]

Scholvinck ML, Maier A, Ye FQ, Duyn JH, Leopold DA. Neural basis of global resting-state fMRI activity. Proc Natl Acad Sci U S A. 2010; 107:10238–10243. [PubMed: 20439733]

Schummers J, Yu HB, Sur M. Tuned responses of astrocytes and their influence on hemodynamic signals in the visual cortex. Science. 2008; 320:1638–1643. [PubMed: 18566287]

Schwinn DA, McIntyre RW, Reves JG. Isoflurane-induced vasodilation: role of the alpha-adrenergic nervous system. Anesth Analg. 1990; 71:451–459. [PubMed: 1977331]

Shmuel A, Leopold DA. Neuronal correlates of spontaneous fluctuations in fMRI signals in monkey visual cortex: Implications for functional connectivity at rest. Hum Brain Mapp. 2008; 29:751–761. [PubMed: 18465799]

Sinclair MD. A review of the physiological effects of alpha(2)-agonists related to the clinical use of medetomidine in small animal practice. Canadian Veterinary Journal-Revue Veterinaire Canadienne. 2003; 44:885–897.

Steriade M, Contreras D, Curro Dossi R, Nunez A. The slow (< 1 Hz) oscillation in reticular thalamic and thalamocortical neurons: scenario of sleep rhythm generation in interacting thalamic and neocortical networks. J Neurosci. 1993a; 13:3284–3299. [PubMed: 8340808]

Steriade M, Nunez A, Amzica F. Intracellular analysis of relations between the slow (< 1 Hz) neocortical oscillation and other sleep rhythms of the electroencephalogram. J Neurosci. 1993b; 13:3266–3283. [PubMed: 8340807]

Steriade M, Nunez A, Amzica F. A novel slow (< 1 Hz) oscillation of neocortical neurons in vivo: depolarizing and hyperpolarizing components. J Neurosci. 1993c; 13:3252–3265. [PubMed: 8340806]

Thompson GJ, Magnuson ME, Merritt MD, Schwarb H, Pan WJ, McKinley A, Tripp LD, Schumacher EH, Keilholz SD. Short-time windows of correlation between large-scale functional brain networks predict vigilance intraindividually and interindividually. Hum Brain Mapp. 2012

Thompson GJ, Merritt MD, Pan WJ, Magnuson ME, Grooms JK, Jaeger D, Keilholz SD. Neural correlates of time-varying functional connectivity in the rat. Neuroimage. 2013

Tian L, Jiang T, Wang Y, Zang Y, He Y, Liang M, Sui M, Cao Q, Hu S, Peng M, Zhuo Y. Altered resting-state functional connectivity patterns of anterior cingulate cortex in adolescents with attention deficit hyperactivity disorder. Neurosci Lett. 2006; 400:39–43. [PubMed: 16510242]

Trimmel M, Mikowitsch A, Groll-Knapp E, Haider M. Occurrence of infraslow potential oscillations in relation to task, ability to concentrate and intelligence. Int J Psychophysiol. 1990; 9:167–170. [PubMed: 2228750]

Trimmel M, Strassler F, Knerer K. Brain DC potential changes of computerized tasks and paper/pencil tasks. Int J Psychophysiol. 2001; 40:187–194. [PubMed: 11228345]

Vincent JL, Patel GH, Fox MD, Snyder AZ, Baker JT, Van Essen DC, Zempel JM, Snyder LH, Corbetta M, Raichle ME. Intrinsic functional architecture in the anaesthetized monkey brain. Nature. 2007; 447:83–86. [PubMed: 17476267]

Waites AB, Stanislavsky A, Abbott DF, Jackson GD. Effect of prior cognitive state on resting state networks measured with functional connectivity. Hum Brain Mapp. 2005; 24:59–68. [PubMed: 15382248]

Weissman DH, Roberts KC, Visscher KM, Woldorff MG. The neural bases of momentary lapses in attention. Nat Neurosci. 2006; 9:971–978. [PubMed: 16767087]

Williams KA, Magnuson M, Majeed W, LaConte SM, Peltier SJ, Hu X, Keilholz SD. Comparison of alpha-chloralose, medetomidine and isoflurane anesthesia for functional connectivity mapping in the rat. Magn Reson Imaging. 2010; 28:995–1003. [PubMed: 20456892]

Zhao F, Zhao T, Zhou L, Wu Q, Hu X. BOLD study of stimulation-induced neural activity and resting-state connectivity in medetomidine-sedated rat. Neuroimage. 2008; 39:248–260. [PubMed: 17904868]

Zornow MH, Fleischer JE, Scheller MS, Nakakimura K, Drummond JC. Dexmedetomidine, an alpha 2-adrenergic agonist, decreases cerebral blood flow in the isoflurane-anesthetized dog. Anesth Analg. 1990; 70:624–630. [PubMed: 1971500]

Highlights

- Local field potential/fMRI coherence can be used to create an effective filter.
- Infraslow field potentials correlate to a spatiotemporal dynamic pattern in fMRI.
- The pattern of time-lagged correlation matches patterns previously observed in fMRI alone.
- Filtered infraslow field potentials weakly correlate with fMRI pattern strength vs. time.
- Results were similar for somatosensory and caudate-putamen regions in the rat brain.

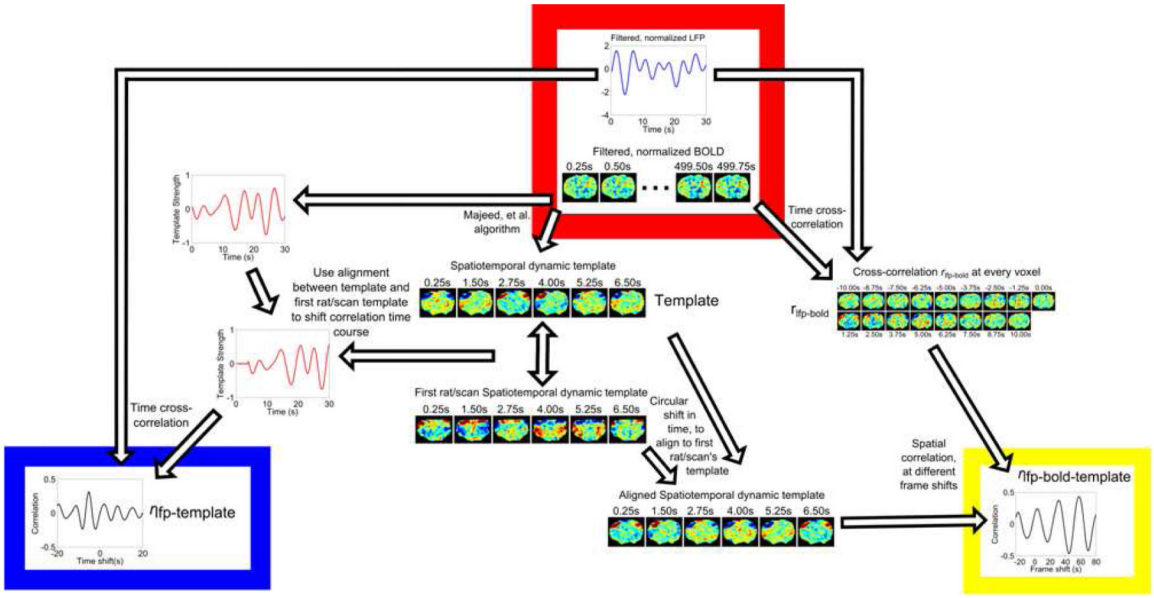

Figure 1.

Summary of the methods used to produce and align $r_{lfp\text{-}bold\text{-}template}$ and $r_{lfp\text{-}template}$. The starting point is highlighted in the red box, with filtered and normalized LFP and BOLD signals. **Right side:** The filtered, normalized BOLD signal is cross-correlated at numerous time lags with the filtered, normalized infraslow LFP signal to produce $r_{lfp\text{-}bold}$. A QPP template is calculated from the filtered, normalized BOLD signal alone. As templates are produced with arbitrary phases, all templates are circularly shifted to align with the first rat, first scan's template for that electrode and anesthesia. Spatial correlation is calculated between the aligned template and $r_{lfp\text{-}bold}$ at several frame shifts to produce $r_{lfp\text{-}bold\text{-}template}$ (yellow box). **Left side:** A QPP template is generated from the filtered, normalized BOLD signal. The algorithm also produces a time course of correlation with the template, which is template strength versus time. As templates are produced with arbitrary phases, all templates are circularly shifted to align with the first rat, first scan's template for that electrode and anesthesia. This shift is used to non-circularly align the phase of the template strength time course. Time cross-correlation is calculated between the aligned template strength time course and the filtered, normalized infraslow LFP signal to produce $r_{lfp\text{-}template}$ (blue box).

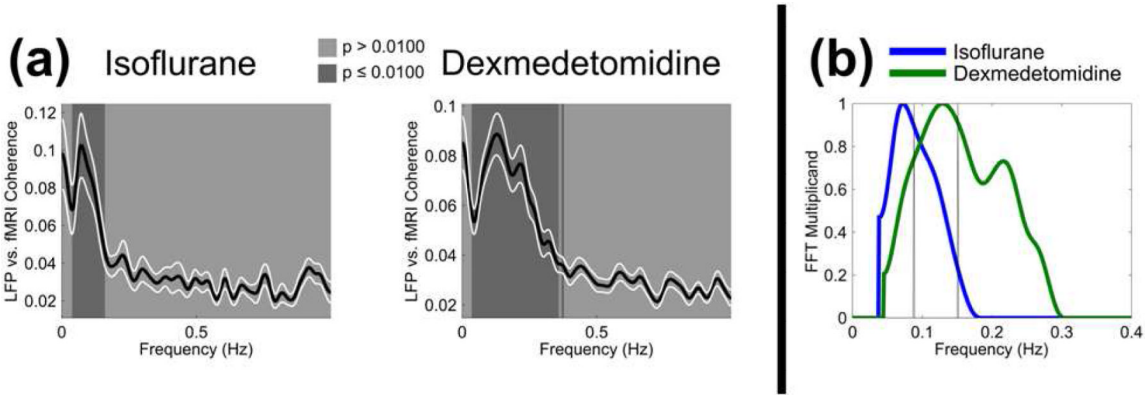

Figure 2.

Significant coherence between infraslow LFP and BOLD produces an empirical filter. **(a)** Magnitude-squared coherence, combined across left and right hemispheres, between infraslow LFP signal recorded from S1FL and BOLD signal from that location. Isoflurane anesthesia is shown on the left, dexmedetomidine on the right. Areas significantly different from randomly shifted pairs are shown in dark gray ($p \leq 0.0100$, SGoF at 5% FWER). **(b)** Empirical filter based on coherence, shown for both anesthesias. The filter is applied as a multiplicand to the fast fourier transform (FFT) of the original signal. The vertical gray line represents the center of mass of each filter. N=92 for dexmedetomidine, 7 rats, 3-14 runs per rat, 2 electrodes. N=34 for isoflurane, 4 rats, 2-8 runs per rat, 2 electrodes.

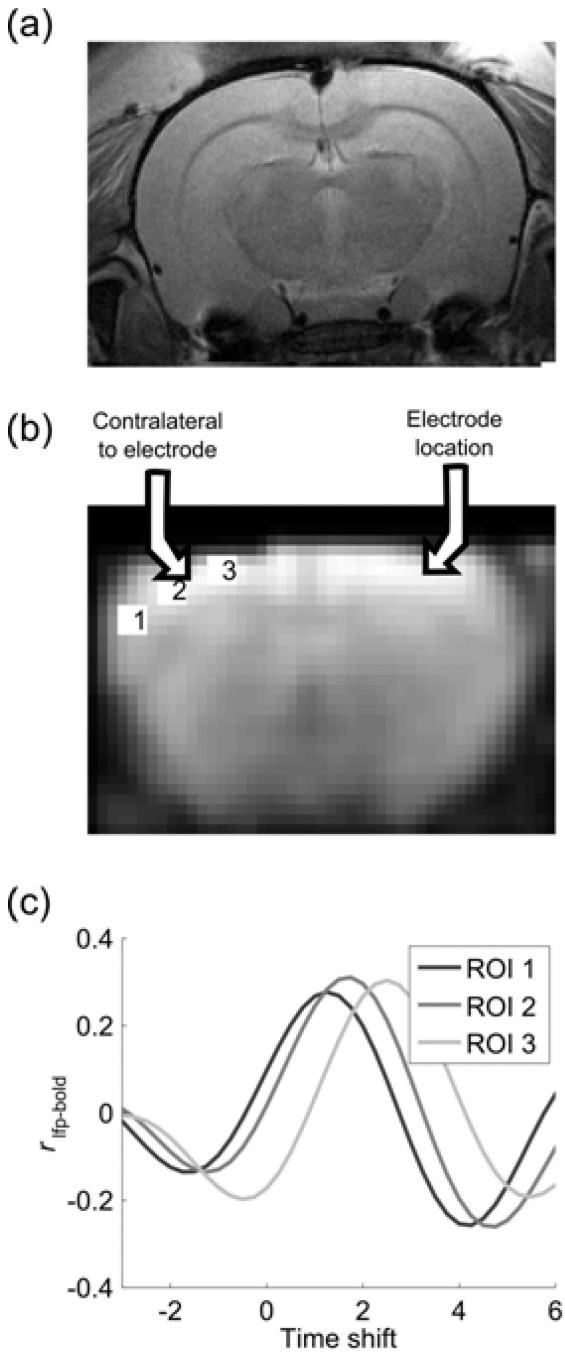

Figure 3.

(a) Anatomical fMRI image of (different) rat brain at slice approximately aligned to BOLD images. **(b)** Mean BOLD image across an fMRI scan, three regions of interest (ROI) are shown numbered. Arrows show approximately the location where the electrodes was implanted (right S1FL) and the contralateral homologue to that region (left S1FL) **(c)** Cross-correlation between the LFP signal at ROI 2 and the BOLD signal at every ROI. Note that the more ventral and lateral ROI 1 peaks at an earlier time shift while the more dorsal and medial ROI 3 peaks at a later time shift. Note also that ROI 2, closest to the contralateral homologue of the site of electrode implantation, has the greatest correlation value of all three regions of interest over the shown time shifts. N = 1; data are from rat 7, scan 5.

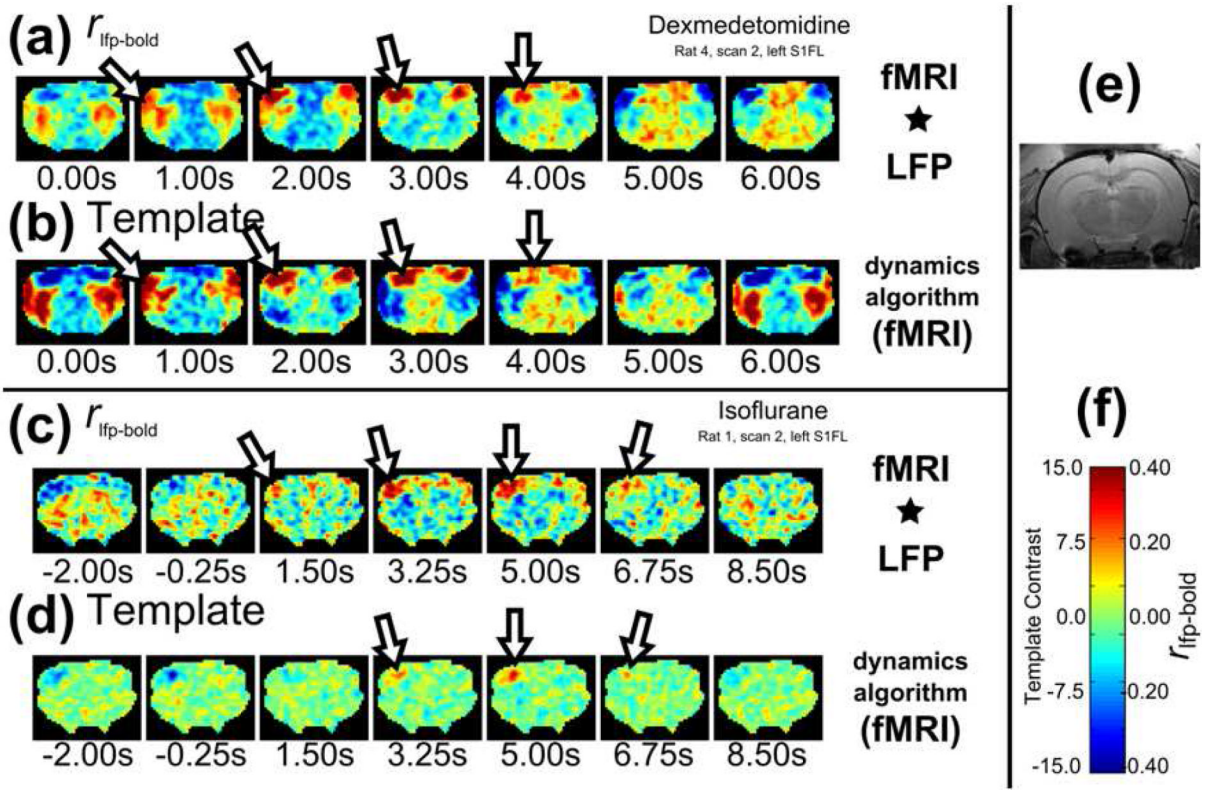

Figure 4.

Examples of spatiotemporal dynamics from LFP-BOLD correlation and QPPs from BOLD signal alone. **(a, c)** Pearson correlation between BOLD and LFP at shown time shifts, $r_{lfp\text{-}bold}$, under dexmedetomidine (a) and isoflurane (c) anesthesia **(b, d)** Template generated from the BOLD signal alone, using the Majeed, et al. algorithm (Majeed et al., 2011) aligned based on the maximum mean spatial correlation between the two patterns shown in Figure 5. Arrows in a, b, c, d show propagation of signal in typical ventral to dorsal direction along cortex. **(e)** Anatomical fMRI image of (different) rat brain at slice approximately aligned to BOLD images. **(f)** Scale bar for a, b, c and d. **Note:** Parts a, b, c, and d are included as movie files in supporting information. N = 1 for each plot, the specific rat/scan/electrode is indicated on the plot.

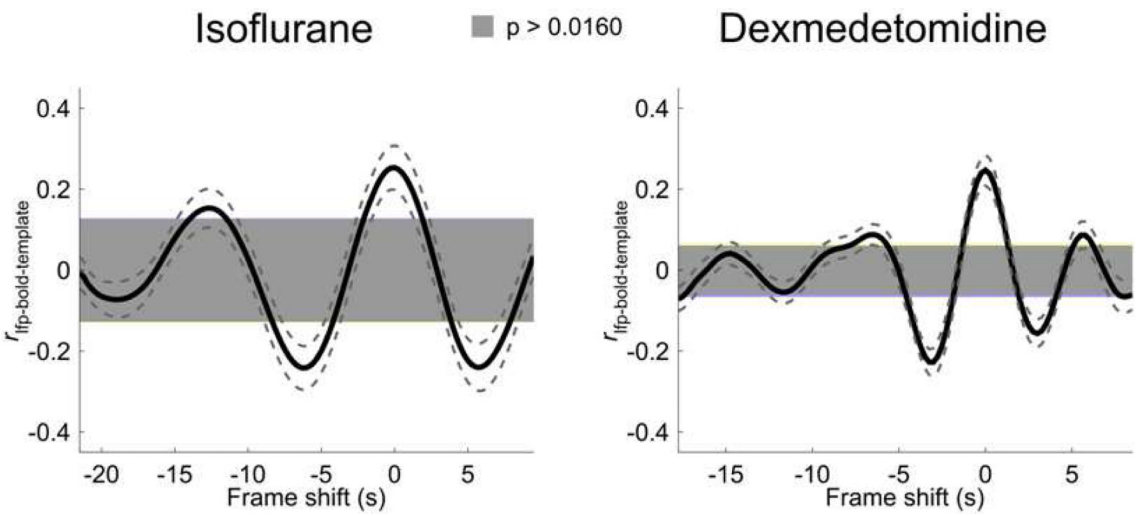

Figure 5.

$r_{lfp\text{-}bold\text{-}template}$; normalized spatial correlation between $r_{lfp\text{-}bold}$ (generated from LFP-BOLD correlation, Figure 4 parts a and c) and QPP templates (generated from BOLD alone, Figure 4 parts b and d) plotted versus frame shift from maximum. Black solid line is mean of all rats and scans, dark gray dashed line is one standard error. Light gray areas are not significant ($p > 0.0160$), other areas are significant (SGoF, 5% FWER). Left is isoflurane anesthesia, right is dexmedetomidine anesthesia. This figure had $r_{lfp\text{-}bold}$ calculated from the left electrode; numerical results from both electrodes are shown in Supplemental table SI, both electrodes and individual rats are shown in Supplemental figure S2. In every case, $r_{lfp\text{-}bold\text{-}template}$ is significant for the largest peak and side peaks, and approximately resembles a down-scaled autocorrelation series. N=46 for dexmedetomidine, 7 rats, 3-14 runs per rat. N=17 for isoflurane, 4 rats, 2-8 runs per rat.

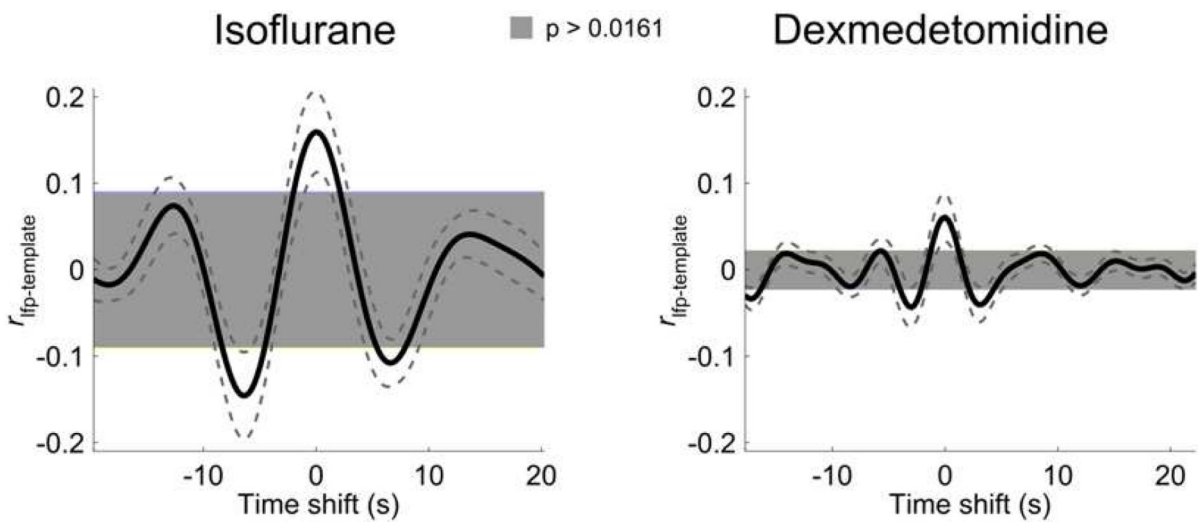

Figure 6.

Pearson correlation between template strength and pre-processed infraslow LFP signal, $r_{\text{lfp-template}}$, plotted versus time shift from maximum. Black solid line is mean of all rats and scans, dark gray dashed line is one standard error. Light gray areas are not significant ($p > 0.0161$), other areas are significant (SGoF, 5% FWER). Left is isoflurane anesthesia, right is dexmedetomidine anesthesia. This figure used data from the left electrode; numerical results from both electrodes are shown in Supplemental table SII, both electrodes and individual rats are shown in Supplemental figure S4. In every case, $r_{\text{lfp -template}}$ is significant for the largest peak and approximately resembles a down-scaled autocorrelation series. N=46 for dexmedetomidine, 7 rats, 3-14 runs per rat. N=17 for isoflurane, 4 rats, 2-8 runs per rat.

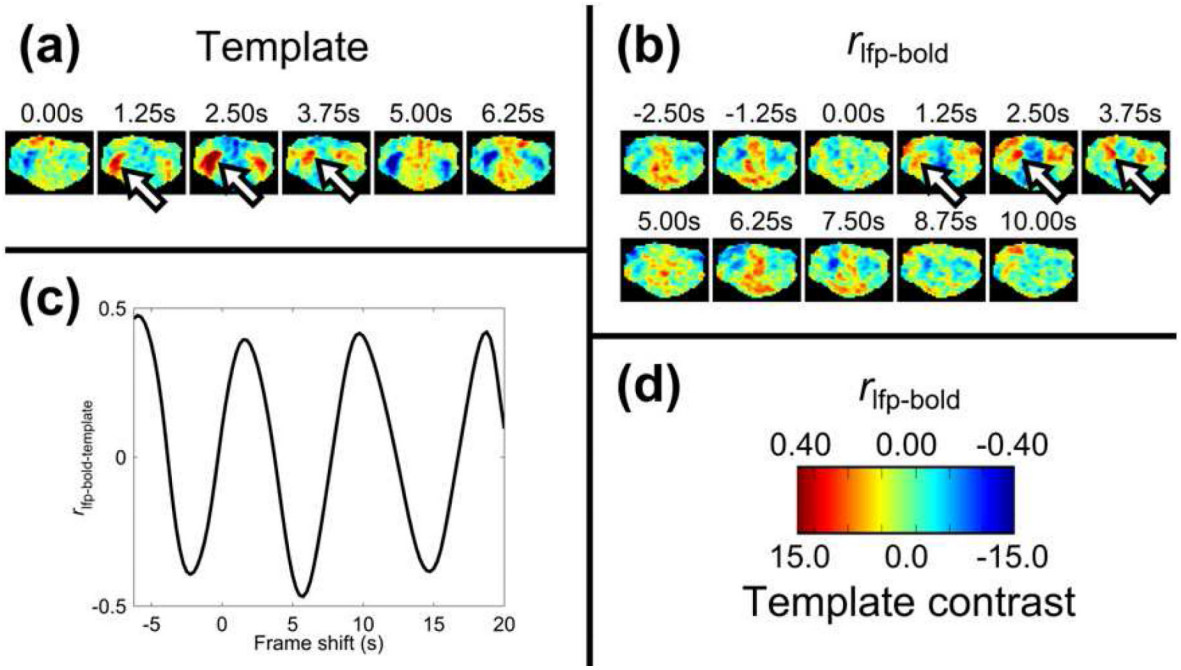

Figure 7.

(a) QPP template generated from BOLD signal alone, using regions of interest in left and right caudate-putamen. Arrows indicate the ventral to dorsal propagation on the side contralateral to the electrode (note it is visible on the ipsilateral side as well). **(b)** Cross-correlation $r_{lfp\text{-}bold}$ between an infraslow LFP signal and the BOLD signal in the caudate-putamen. Arrows indicate the ventral to dorsal propagation on the side contralateral to the electrode (note it is visible on the ipsilateral side as well). **(c)** Spatial correlation $r_{lfp\text{-}bold\text{-}template}$ between $r_{lfp\text{-}bold}$ from (b) and the template from (a). **(d)** Scale bar for (a) and (b). Parts (a) and (b) are included as movie files in supporting information. N=1. As some rats had $r_{lfp\text{-}bold\text{-}template}$ similar to this (Supplemental figure S2), it is possible that by using more scans and rats, that this would appear more like an autocorrelation series. It is also possible that an empirical filter generated from the caudate-putamen region instead of the S1FL region would make this result more consistent with what was observed in S1FL.

Table I

This table illustrates mean and one standard deviation (SD) for maximum $r_{lfp\text{-}bold}$, cross-correlation between infraslow LFP and BOLD signals in S1FL and the time shift to this maximum correlation value.

	Isoflurane				Dexmedetomidine			
	Time shift		Value		Time shift		Value	
	Mean	SD	Mean	SD	Mean	SD	Mean	SD
Standard Filter	1.5s	±4.5s	$r_t = 0.52$	±0.13	1.2s	±4.4s	$r_t = 0.47$	±0.10
Empirical Filter	3.1s	±2.5s	$r_t = 0.51$	±0.1	2.0s	±2.6s	$r_t = 0.40$	±0.08

Values for both a standard filter (0.005-0.1Hz boxcar, (Liu et al., 2010)) and an empirically generated filter (Figure 2 b) are shown. In every case the standard deviation is higher for the standard filter, in particular the standard filter does not produce a reproducible time shift between infraslow LFP and BOLD. For both filters, a significant difference in anesthetics was seen in terms of maximum $r_{lfp\text{-}bold}$ value ($p = 3.08\times10^{-2}$ for standard filter, $p = 7.69\times10^{-9}$ for empirical filter, two sample T tests) and for the empirical filter a significant difference in anesthetics was seen in terms of the infraslow LFP-BOLD time shift that resulted in maximum $r_{lfp\text{-}bold}$ ($p = 3.10\times10^{-2}$, two sample T test). The significant difference in time shifts between anesthetics is not the focus of this study (see *4.4*) but replicates previous work (Pan et al., 2013). The large difference between the mean time shifts for the two filters is likely due to the large error in terms of this time shift that was seen in the standard filter (1.8-2.0 seconds greater standard deviation than the empirical filter). N=46 for dexmedetomidine, 7 rats, 3-14 runs per rat. N=17 for isoflurane, 4 rats, 2-8 runs per rat.

Table II

Visual observation of dynamics in correlation between BOLD and LFP ($r_{lfp\text{-}bold}$). The number shown is total number of that dynamic observed, out of the total number of observations, including observation of both hemispheres, both electrodes, all rats and all scans.

	Positive/Negative Alternation	Cortical ventral-dorsal propagation	Cortical dorsal-ventral propagation
Isoflurane	66/68 (97.1%)	35/68 (51.5%)	6/68 (8.82%)
Dexmedetomidine	180/184 (97.8%)	127/184 (69.0%)	22/184 (12.0%)